CO6-1

Development of Boron Cluster-Loaded Nanoparticles for BNCT

A.B. Fithroni, S. Zhou, T.F.N. Hakim, T. Tada, M. Suzuki[2], Y. Sakurai[2], N. Yamada[3], K. Watanabe, T. Ohtsuki, and E. Matsuura[1,4]

Department of Interdisciplinary Science and Engineering in Health Systems, Okayama University
[1]Collaborative Research Center for OMIC, Graduate School of Medicine, Dentistry, and Pharmaceutical Sciences, Okayama University
[2]Institute for Integrated Radiation and Nuclear Science, Kyoto University
[3]Nihon Fukushi Fuiin Holding, Co., Ltd.
[4]Neutron Therapy Research Center (NTRC), Okayama University

INTRODUCTION: Boron neutron capture therapy (BNCT) is a less-invasive nuclear therapeutic approach that highly selective to induce cancer apoptosis, without any cytotoxic effects in neighboring cells [1]. BPA and BSH as current clinically approved boron compounds have several limitations related to selectivity and effectivity [2]. To address the issues, a novel self-forming nanoparticle, which is consisted of biodegradable polymers, namely, "Lactosome" with a hydrophobic boron cluster have been developed [3]. In the previous study, the BNCT effects were successfully obtained after exposing neutron irradiation to the AsPC-1 cells (human pancreatic cancer cells) in vitro and in vivo [4]. In this study, we compared in vitro BNCT effect on a boron cluster loaded with different type of Lactosome "type 1" and "type 2" particles.

EXPERIMENTS: For in vitro study, AsPC-1 cells were subjected to irradiation at reactor power 1 MW for 10 min or 40 min after 2 hr incubation with boron cluster-loaded Lactosome particles. After the neutron irradiation, the cells were cultured in 12-well plates and incubated under 5% CO_2 at 37 °C for 14 days. Then, colony formation assay was performed after staining.

RESULTS: In vitro irradiation showed that Lactosome loaded with boron cluster significantly inhibited the AsPC-1 cells growth. Interestingly, Lactosome "type 1" particles loaded with boron cluster showed significant inhibition as compared to Lactosome "type 2" ones loaded with boron cluster after irradiation for 10 min. Moreover, both types of Lactosome particles loaded with boron cluster respectively showed remarkable inhibition of cancer cells at 40 min. Overall, in vitro irradiation study showed that both type of Lactosome loaded with boron cluster respectively are promising candidates for BNCT.

Table 1 In vitro inhibitory effect of AsPC-1 cells treated with Lactosome particles loaded with boron clus-ter.

Group	Colony formation rate		
	0 min	10 min	40 min
Control (DPBS)	1	0.82 ± 0.14	0.42 ± 0.08
Lactosome "type 1"	1	0.90± 0.09	0.33± 0.04
Lactosome "type 2"	1	1.00± 0.12	0.42± 0.04
Lactosome "type 1" loaded with boron cluster	1	0.03± 0.05	0.03± 0.02
Lactosome "type 2" loaded with boron cluster	1	0.25± 0.09	0.01± 0.00

REFERENCES:
[1] M. Suzuki. Int. J. Clin. Oncol., **25** (2020) 43-50.
[2] J.H. Goodman*et al.,* Neurosurgery, **47** (2000) 608-621.
[3] A.B. Fithroni *et al.,* Cells, **11** (2022) 3307.
[4] A.B. Fithroni *et al.,* Cells, **14** (2025) 60.

CO6-2

Mechanism of amyloid fibril formatin by serum amyloid protein A

T. Okunishi[1], K. Morishima[2], R. Inoue[2], M. Sugiyama[2] and M. Hoshino[1]

[1]*Graduate School of Pharmaceutical Sciences, Kyoto University*
[2]*Institute for Integrated Radiatio n and Nuclear Science, Kyoto University*

INTRODUCTION: Systemic amyloidosis is the protein-misfolding disease characterized by the deposition of amyloid fibril-forming proteins in multiple organs. Fibril formation by serum amyloid A (SAA), 104 amino acid residue protein, could cause systemic AA amyloidosis. SAA is a kind of apolipoprotein, which contribute to the formation of high-density lipoprotein (HDL), and plays a vital role in the transport of lipids and cholesterol in the blood. The HDL is mainly composed of apolipoprotein AI (apoA-I), and the concentration of SAA is usually low (≤ 10 μg/mL). However, in the acute phase, its serum level increases approximately 1000-fold under the action of inflammatory cytokines. The remarkable elevation of its serum level is considered to a risk factor of amyloid deposition.

EXPERIMENTS: The fusion protein of histidine-tagged ubiquitin and serum amyloid A (H6UbSAA), and yeast ubiquitin hydrolase-1 (YUH-1) were expressed by Escherichia coli strain BL21(DE3)-Gold. The protein expression was induced by isopropyl b-D-thiogalactopyranoside (IPTG). The protein was purified with histidine affinity chromatography, followed by the proteolytic digestion at the C-terminus of ubiquitin by YUH-1. The digested purified by reverse-phase HPLC with a linear gradient of acetonitrile, and SAA moiety was collected. Circular dichroism (CD) spectra were measured using Jasco J-820 spectropolarimeter with 1-mm light path length at protein concentration of 20 μM. Amyloid fibrillation was monitored as the increase in fluorescence of thioflavin T (ThT). After the incubation of protein at 20 μM and 37°C for the indicated time, an aliquot (66.7 μL) was added to 1.93 mL of 5 μM ThT. Fluorescence at 490 nm was measured at an excitation wavelength of 446 nm on a Shimadzu RF-5300 spectrofluorometer.

RESULTS: We analyzed the secondary structure of SAA at 4°C and 37°C by far-UV CD spectroscopy (Figure 1A). The spectrum at 4°C showed typical double minima at 222 and 208 nm, suggesting that the protein assumed mostly α-helical conformations. On the other hand, the spectrum recorded at 37°C was significantly different from that at 4°C and the signal intensity decreased significantly. Next, we examined the amyloid fibril formation by SAA1 at 4°C and 37°C (Fig1B). We found that the protein spontaneously formed ThT-active aggregates at 37°C. On the other hand, such a spontaneous fibril formation was not observed at 4°C. The results suggested that the fibril formation was closely related to the structure of the protein, and the loss of α-helical secondary structure seems to be the prerequisite for amyloid fibrillation by SAA1.

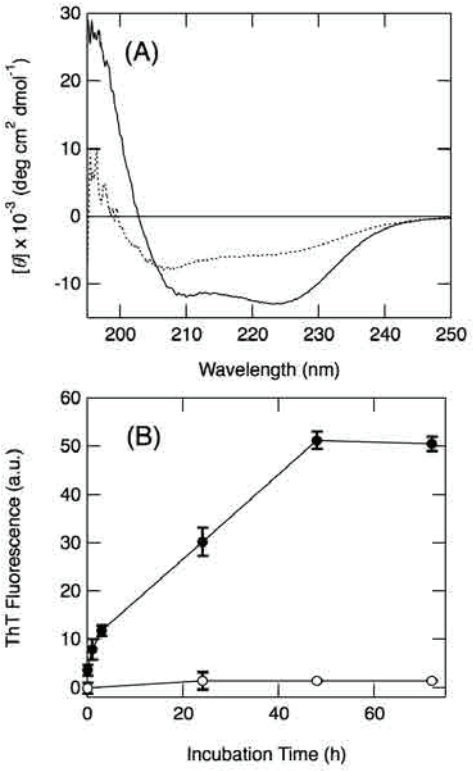

Fig. 1 (A) Far-UV CD spectra of SAA1 at 4°C (solid) and at 37°C (dotted) (B) Change in the ThT-fluorescence after the incubation at 4°C (open cicle) and at 37°C (closed circle)

CO6-3

Multi Element Neutron Activation analysis in the Gum Samples of the Diet of Small Primates

M. Fukushima, Y. Iinuma[1], H. Imai[2], Y. Tsuji

Faculty of Science and Engineering, Ishinomaki Senshu University
[1]Institute for Integrated Radiation and Nuclear Science, Kyoto University
[2]Center for the Evolutionary Origins of Human Behavior, Kyoto University

INTRODUCTION: Calcium is one of the essential ion to make bone and reproductive physiology of animals. Callithrix primates tend to consume plant extrudes which is known as high calcium. In this study four different natural gum samples and Arabic gum sample (purchased) were analyzed by neutron activation analysis (NAA) for eight element levels in them. Calcium levels were compared with the results obtained by colorimetric method.

EXPERIMENTS: Four different gum samples were extracted from Siniguena (Spondias purpurea), Barauna (Schinopsis brasiliensis), Algaroba (Prosopsis juliflora), and Ansico (Anadenanthrera macrocarpa). Gum samples except Arabic gum sample were extracted, freeze dried, and pulverized for further experiment. One portion of dried power was supplied for short irradiation in KUR. Eight elements of Ca, Cl, Cu, K, Mg, Mn, Na, and V were analyzed by the condition of TcPn irradiation (1.5 min. irradiation, 3.0 min. cooling, 10 min gamma counting by Ge detector with Compton suppression system). Colorimetric method for analyzing calcium was done by using QuantiChrom Assay kit (BioAssay Systems), absorbance at 612 nm of gum sample aquatic solutions were measured, and Ca levels were calculated from the standard curve.

RESULTS: Elemental levels obtained for the gum samples are shown in Table 1. Also, levels of Ca in the gum samples are shown in Fig. 1. There are variations of the Ca concentration between the gums. Interestingly, some of the gum (A, D) showed higher concentration when measured by NAA compared to the results of colorimetric method.

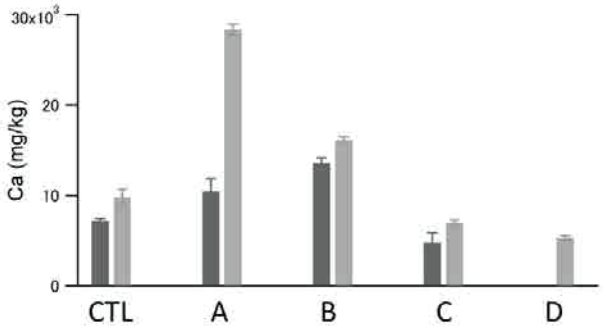

Fig. 1. Ca levels in the gum samples measured by the methods of chrorimetric (black) and neutron activation analysis (gray). CTL sample is Arabic gum, and natural gums from (A) Siniguena (*Spondias purpurea*) (B) Barauna (*Schinopsis brasiliensis*) (C) Algaroba (*Prosopsis juliflora)* (D) Ansico (*Anade-nanthera macrocarpa*) are shown.

Table 1. Elemental levels in gum samples (unit: mg/kg, dry weight).

	Mg	Cu	Na	V	K	Cl	Mn	Ca
Arabic gum	2390				9310			9760
Siniguela	1850		226	0.19	1140	128		28400
Barauna	1760		91		2490		39.7	16100
Algaroba	1020	22	474		9230	1090	38.0	7010
Ansico	627		153		7650		20.7	4320

These results suggest the presence of insoluble fraction of Ca in some gum which would appear after the fermentation of gum in the cecum.

REFERENCES:

[1] M. L. Power S D Tardif, D G Layne, J Schulkin, Am. J. Primatol., **47** (1999) 255-261.
[2] H. Imai, N. Suzuki, Y. Ishimaru, T. Sakurai, L. Yin, W. Pan, K. Abe, T. Misaka, H. Hirai, Biology letters, **8** (2012) 652-656.
[3] Y. Maruyama, R. Yasuda, M. Kuroda, Y. Eto, PLoS ONE, **7** (2012) e3448.

CO6-4

Quantitative Determination of a Neutron-sensitizing reagent, *p*-Borono-L-phenylalanine (BPA), Absorbed in Rice Seeds by Prompt Gamma-Ray Analysis

Y. Hattori, T. Kinouchi[1], S. Segami[2], and M. Kirihata

Research Center of Boron Neutron Capture Therapy, Osaka Metropolitan University, Japan
[1] Institute for Integrated Radiation and Nuclear Science, Kyoto University, Japan
[2] Research Institute of Environment, Agriculture and Fisheries, Osaka Prefecture, Japan

INTRODUCTION: In boron neutron capture therapy (BNCT), the efficient absorption of boron-10 (^{10}B) compounds, as neutron sensitizers, by tumor cells determines their clinical effect. BPA, *p*-borono-L-phenylalanine, is a primary ^{10}B compound in BNCT because it effectively delivers to tumor cells and induces DNA double-strand breaks (DSBs) in the cells by the BNC reaction. In recent studies, we have attempted to apply these properties of the combination of BPA and BNC reaction to crop breeding. In the case of BNCT, the induction of a large number of DSBs produces an anti-tumor effect, but if a small number of DSBs is generated, it leads to genetic mutation, which implies selective breeding. Therefore, we first attempted to absorb BPA in rice seeds and measure the amount of absorbed BPA by prompt gamma-ray analysis.

EXPERIMENTS: Preparation of BPA-absorbed rice seeds> Unhulled rice seeds were immersed in BPA solution (300 ppm) for 24 hours. After drying, the rice seeds were solubilized sequentially by dry and wet ashing treatments. Dry ashing was performed in an electric oven at 550°C for 5 hours. For wet ashing, the ashed samples were placed in a mixture of 68% (w/w) nitric acid and 30% (w/w) hydrogen peroxide water at 7:3 and decomposed using MARS 6, a microwave digestion system, at 210°C for 30 minutes.
Prompt gamma-ray analysis for ^{10}B determination in BPA-absorbed rice seeds > Solubilized rice seeds were irradiated by thermal neutrons during 600 sec at E-3 irradiation port of KUR under 5 MW operation to demonstrate the measurement of 478 keV prompt gamma rays.

RESULTS: After preparing a calibration curve of the ^{10}B concentration by boron standard solution, the concentration of ^{10}B in the blank group, consisting of only ultrapure water, the control group, in which only ultrapure water was absorbed by unhulled rice seeds, and the experimental group, in which BPA was absorbed, was measured by E-3 irradiation port. As shown in Table 1, all measured values were negative in the control group, and in some cases, the values were also negative in the BPA-treated group. This phenomenon was observed repeatedly, even when the BPA concentration was increased to 1,000 ppm. On the other hand, because alpha-ray autoradiography using CR-39, a solid-state nuclear tracking detector, visualizes that BPA absorbed by rice seeds accumulates in their embryo and outer coat, there is no doubt that the rice seeds absorb BPA (cf. R6142). Therefore, some obstacles might exist in measuring the ^{10}B concentration in the rice seeds by prompt gamma-ray analysis.

Sample category	Sample No.	^{10}B conc.
Blank	1	0.007
	2	0.007
	3	0.032
Control	1	-0.050
	2	-0.075
	3	-0.320
	4	-0.419
	5	-0.492
BPA (300 ppm)	1	0.122
	2	-0.173
	3	0.147
	4	-0.075
	5	0.147
	6	-0.615

Table 1. ^{10}B concentration in rice seeds: Each sample's estimated ^{10}B conc is in ppm. Sample No. indicates several independent trial samples.

CO6-5

Structural analysis of surfactant-induced α-synuclein protofibrils by small-angle X-ray scattering combined with analytical ultracentrifugation

S. Kitano, K. Morishima[1], R. Inoue[1], M. Sugiyama[1], E. Chatani

Graduate School of Science, Kobe University
[1]Institute for Integrated Radiation and Nuclear Science, Kyoto University

INTRODUCTION: Amyloid fibrils are protein aggregates involved in amyloidoses and neurodegenerative diseases. In the early stages of their formation, oligomers and protofibrils have been identified, particularly in neurodegenerative diseases. These aggregates are suggested to be the main culprits of cellular toxicity rather than mature amyloid fibrils; however, their physicochemical properties have still been awaiting clarification. Referring to a previous report [1], we have focused on the formation of α-synuclein protofibrils in the presence of sodium dodecyl sulphate (SDS) and investigated their structural properties by using small-angle X-ray scattering (SAXS) and analytical ultracentrifugation (AUC).

EXPERIMENTS: A recombinant α-synuclein protein was prepared and dissolved at a final concentration of 2.0 mg/mL in 25 mM Tris-HCl buffer (pH7.4) containing 100 mM NaCl, 1 mM ethylenediamine-N,N,N',N'-tetraacetic acid, and 0.5 mM SDS. The sample was incubated at 37 °C for 24 hours in quiescence to proceed the formation of protofibrils. The samples were then subjected to SAXS and AUC measurements to investigate the size distribution and averaged shape of the aggregates formed. SAXS profiles were measured at 25 °C and 30-minute exposure time by a NANOPIX equipped with a HyPix-6000 (Rigaku Corporation). A Cu K-α line (MicroMAX-007HFMR) was used as a beam source, which was further focused and collimated with a confocal multilayer mirror (OptiSAXS). AUC data were obtained at 25 °C and 40000 rpm with a ProteomeLab XL-I analytical ultracentrifuge (Beckman Coulter) and analyzed using SEDFIT based on a sedimentation velocity protocol.

RESULTS: The SAXS profile of the protofibril sample exhibited a characteristic scattering pattern with intensity intermediate between those of monomers and of amyloid fibrils (Fig. 1A, orange). The slope of the I(q) at low q region was close to −1, showing the rod-like shape of protofibrils. Although the fraction of protofibrils was only 1%, which was revealed from the AUC analysis, it was confirmed that the unreacted α-synuclein monomers had negligible effects and there was little change in the profile after subtracting their contribution (Fig. 1A, red). Using cross-sectional Guinier plot (Fig. 1B), the diameter of protofibril was calculated to be approximately 15 nm. It has been suggested that SAXS is a powerful technique to identify and characterize protofibrils, which is available even when protofibril population is small.

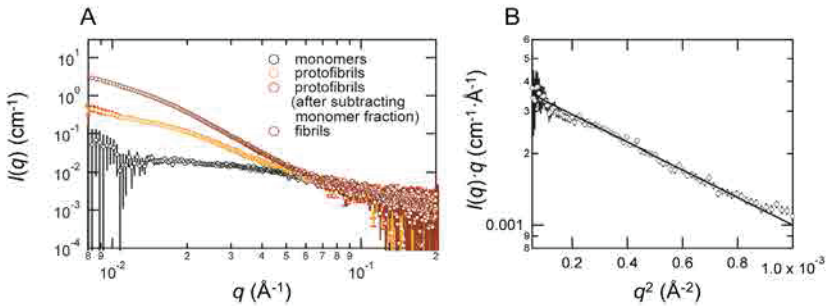

Fig. 1. SAXS profile (A) and its cross-sectional Guinier plot (B) of the α-synuclein protofibrils formed in the presence of 0.5 mM SDS. In panel A, the profiles of α-synuclein monomers and amyloid fibrils are also shown.

REFERENCE:

[1] L. Giehm *et al.*, J. Mol. Biol. **401** (2010) 115-133.

CO6-6

Neutron activation of gold complex

A. Toyoshima, K. Kajiyama[1], M. Murakami, A. Mitsukai[2], and J. Kataoka[3]

Institute for Radiation Sciences, Osaka University
[1]School of Science, Osaka University
[2]Graduate School of Science, Osaka University
[3]Graduate School of Advanced Science and Engineering, Waseda University

INTRODUCTION: Radiopharmaceuticals play a vital role in both the diagnosis and treatment of cancer. They are conventionally synthesized via chemical labeling, in which a medically applicable radioisotope, produced using a nuclear reactor or an accelerator, is attached to a precursor molecule. In this study, we propose a novel methodology for the direct synthesis of radiopharmaceuticals through neutron activation in a reactor. When a stable isotope within a precursor molecule is irradiated with thermal neutrons, prompt gamma rays are emitted following a neutron absorption reaction. This causes nuclear recoil of the activated atom, which may alter molecular structure and affect the chemical integrity of the molecule. Previously, we have investigated this approach using gold nanoparticles (AuNPs). Under specific irradiation conditions, dried AuNP samples were successfully re-dissolved after activation and used in subsequent animal experiments. In the present study, we extend this approach to examine the structural stability of a gold complex, Auranofin, following neutron activation.

EXPERIMENTS: A weighted amount of Auranofin was dissolved in acetone. An aliquot corresponding to 0.1 mg of Auranofin was transferred into a quartz tube and was dried by solvent evaporation. After evaluating the interior, the tube was sealed. Neutron irradiation was conducted for one hour at the Kyoto University Research Reactor. The irradiated sample was then recovered by dissolving it in 1 mL of acetone, followed by drying and re-dissolution in 0.5 mL of acetonitrile. High performance liquid chromatography (HPLC) was used to analyze the Auranofin sample. The HPLC system was equipped with a series of UV and NaI detectors to identify non-activated compounds and to detect gamma-ray, respectively.

RESULTS: The radioactivity of ^{198}Au produced by neutron irradiation was determined using a Ge detector to be 2.4±0.1 MBq on average. The activated Auranofin was quantitatively recovered in acetone. HPLC analysis showed that main peak of ^{198}Au has the same retention time as that detected with the UV detector. This indicates that the ^{198}Au peak attributes to activated Auranofin. Minor ^{198}Au peaks were also observed, probably suggesting that decomposed by-products are formed by nuclear recoils.

CO6-7

Study on the Amyloid Fibril Disaggregation Mechanism of Hsp104 from *Chaetomium thermophilum*

M. Yohda[1], K. Noi[1,2], K. Shibata[1], Y. Goto[1], M. Matsui[1], M. Hayata[1], K. Shinohara[1], K. Morishima[3], R. Inoue[3], M. Sugiyama[3]

[1]*Department of Biotechnology and Life Science, Tokyo University of Agriculture and Technology*
[2]*Engineering Biology Research Center, Kobe University*
[3]*Institute for Integrated Radiation and Nuclear Science, Kyoto University*

INTRODUCTION: Neurodegenerative diseases, such as Parkinson's disease, are thought to result from the deposition of abnormally aggregated proteins in various tissues. Molecular chaperones are considered potential biological inhibitors that counteract the formation of such aggregates. Among these chaperones, Hsp104 has demonstrated the ability to disaggregate protein aggregates and reduce their cytotoxicity. Hsp104, along with its bacterial homolog ClpB, forms hexameric ring structures that mediate protein disaggregation [1]. It is believed that the disaggregated polypeptide threads through the central channel of the ring. However, the detailed mechanism underlying the disaggregation process remains unclear. We have been investigating the protein disaggregation mechanism of Hsp104 from Chaetomium thermophilum (CtHsp104) [2]. In this study, we examined its reactivity toward various pathogenic amyloid fibrils derived from human α-synuclein, Huntingtin (Htt)/PolyQ, and insulin.

EXPERIMENTS: Wild-type and N-terminal deletion mutant forms of CtHsp104 were expressed in E. coli and purified using anion exchange chromatography, hydrophobic interaction chromatography, and gel filtration chromatography. Human α-synuclein and Huntingtin (Htt)/PolyQ were also expressed in E. coli and purified by affinity chromatography. Human insulin was purchased commercially. Amyloid fibril formation was confirmed by atomic force microscopy (AFM) and by monitoring changes in Thioflavin T fluorescence. Real-time disaggregation was directly visualized using high-speed AFM.

RESULTS: When wild-type (WT) CtHsp104 and its N-terminal deletion mutant (ΔN) were each added to amyloid fibrils and incubated at room temperature for 2 hours, a reduction in fibril content was observed for both α-synuclein and Htt/PolyQ fibrils compared to the control. However, no reduction was observed in insulin fibrils. Next, the disaggregation activity of Hsp104 was evaluated using Thioflavin T fluorescence. After allowing sufficient time for fibril formation, samples of α-synuclein, Htt/PolyQ, and insulin fibrils were incubated with CtHsp104 WT and ΔN, and fluorescence intensity was monitored over a 2-hour period. A time-dependent decrease in fluorescence was observed for α-synuclein and Htt/PolyQ fibrils compared to the control. In contrast, no significant change in fluorescence was observed for insulin fibrils. Finally, real-time disaggregation was directly visualized using high-speed atomic force microscopy (AFM). This analysis revealed that CtHsp104 WT was capable of fragmenting and disaggregating α-synuclein and Htt/PolyQ fibrils. These results suggest that CtHsp104 can disaggregate α-synuclein and Htt/PolyQ fibrils, but may not be effective against insulin fibrils, indicating that Hsp104 exhibits substrate-specific activity depending on the chemical stability of each amyloid fibril. Furthermore, the data indicate that CtHsp104 can disaggregate α-synuclein and Htt/PolyQ fibrils independently, without the need for additional cofactors. In addition, the findings suggest that, in fungal Hsp104—as opposed to the yeast-derived Hsp104 previously studied by other groups—the N-terminal domain may not be essential for amyloid fibril disaggregation.

REFERENCES:

[1] J.R. Glover *et al.,* Cell, **94** (1998) 73-82.
[2] Y. Inoue *et al.,* Structure, **29** (2021) 721-730.

CO6-8

Visualization of intrinsically disordered structure of F_1-ATPase ε subunit through integration of AUC-SAXS measurement and MD simulation

T. Oroguchi[1], K. Morishima[2], R. Inoue [2], M. Sugiyama[2], Y. Yamada[3]

[1] Department of Physics, Faculty of Science and Technology, Keio University
[2] Institute for Integrated Radiation and Nuclear Science, Kyoto University
[3] Department of Life Science, College of Science, Rikkyo University

INTRODUCTION: The ε subunit of F_oF_1-ATPase synthase plays as an intrinsic regulator of ATPase activity of F_1-ATPase depending on ATP concentration. The C domain of this subunit is an intrinsically disordered region, and the specific binding to ATP induces the structural formation of this domain and switches the inhibitory state off [1,2]. Furthermore, it has been recently reported that the disordered structure of the ε subunit is also involved in regulating the rotational coupling between F_o and F_1-ATPase [3]. Therefore, to elucidate the regulatory mechanism by the ε subunit, it is necessary to visualize its disordered structure. However, such visualization is difficult for the existing structural analyses methods such as X-ray crystal structure analyses, cryo-electron microscopy, etc. In this study, we challenge to visualize the disordered structure of the ε subunit through the technique integrating SAXS experiments and MD simulation [4]. Due to its tendency to aggregate, the ε subunit was measured using AUC-SAXS [5], which allows to confirm oligomeric states during measurement.
****

EXPERIMENTS: We condensed the purified isolated ε subunit to a concentration of 4 mg/ml, where SAXS intensity could adequately obtained, and conducted AUC-SAXS measurements. The measurements were conducted for both the ATP-unbound and the ATP-bound states. The ionic strength of the measurement buffer was adjusted to 150 mM to minimize aggregation.
****

RESULTS: Through the measurements from the last year, we were able to observe the structural change of the ε subunit due to ATP binding. The SAXS data revealed that the adopted condensation protocol and measurement conditions allowed us to obtain the non-aggregated ε subunit. The measurements in the last year revealed that the ε subunit exists in a monomer-dimer equilibrium for both ATP-unbound and ATP-bound states. Therefore, we surveyed the solution condition, in which we can obtain the data for monomer state. Then, we succeeded to obtain the data for the monomer state for ATP-unbound state, which is under analysis by MD simulation. For ATP-bound state, we elucidated the monomer-dimer equilibrium (Fig. 1(A)), and succeeded to account for the AUC-SAXS data by MD simulation (Fig. 1(B)).
****

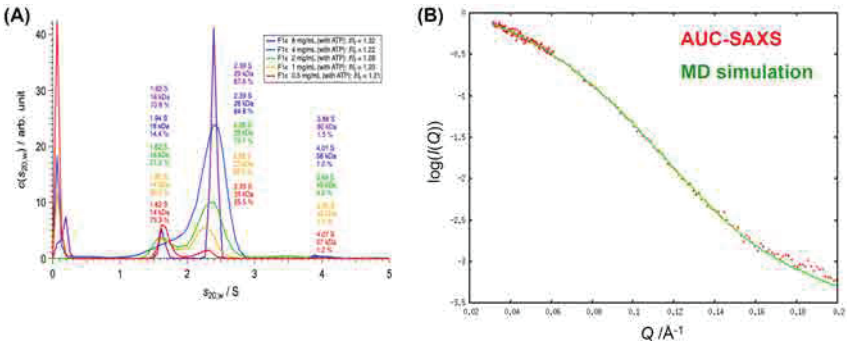

Fig. 1 (A) AUC data for the ATP-bound state of the ε subunit. (B) Comparison of SAXS and MD data.

REFERENCES:

[1] Y. Kato-Yamada & M. Yoshida, J. Biol. Chem., **278** (2003) 36013-36016 .
[2] S. Kato, M. Yoshida & Y. Kato-Yamada, J. Biol. Chem., **282** (2007) 37618-37623.
[3] F. Kadoya, S. Kato, K. Watanabe & Y. Kato-Yamada, Biochem. J., **437** (2011) 135-140.
[4] T. Oroguchi *et al.,* Biophys. J., **96** (2009) 2808-2822.
[5] K. Morishima *et al.,* Comm. Biol., **3** (2020) 294.

CO6-9

Evaluation of oxidized lens βB2-crystallins involved in age-related cataract

T. Takata, J. Sun and K. Lampi[1]

Institute for Integrated Radiation and Nuclear Science, Kyoto University
[1] Oregon Health & Science University

INTRODUCTION: The transparency of the lens is maintained by the stable long-lived protein interactions, comprising three kinds of crystallin families. Those proteins are very stable, but are decreased their stability with age. A kind of intrinsic damages of lens crystallins, such as heat damage, or extrinsic damages such as UV damage are increased with life time. Several researches suggested the amount of heat/UV damage on lens crystallins could be well described by the amount of modifications of amino acid residues [1]. Oxidation is one of the primary damages for crystallins after heat/UV exposure. In this year, we would like to examine investigating distribution of oxidation of tryptophan residues (Trp: W) in lens βB2-crystallins of different sizes after gamma-ray irradiation. Due to the technical troubles, we could not perform quantitative analysis of modifications depending on the each size of oligomer. However, all of five Trps had oxidation even in lower irradiated samples. Therefore, we focused on the result of oxidations and analyzed the contributions of oxidations for lens βB2-crystallins structure/stabilities.

EXPERIMENTS: Due to the structural similarity between oxidative derivatizes of Trp and phenylalanine (Phe: F), five Trp residues in βB2-crystallin were replaced by Phe respectively to simulate the oxidation effect of Trp in βB2-crystallin by site-directed mutagenesis (W59F, W82F, W85F, W151F and W196F). Each sample were prepared to 4.0 mg/mL in 50 mM Tris buffer (pH 7.8), 150 mM NaCl, and were injected into the Superdex™ 200 Increase 10/300 column equipped on an AKTA GO purifier system (Cytiva) at the Institute for Integrated Radiation and Nuclear Science, Kyoto University.

RESULTS: All mutants, except for W151F, showed a huge peak for dimer and a small peak for tetramer; W151F only showed a peak for dimer. Comparison of the peak area of the tetramer and dimer for each showed that W59F formed more tetramers than the other samples (Fig. 1). Shoulder peaks in the W59F chromatogram were indicative of multiple oligomeric states. Those results are consistent with previous studies that W59 are critical to βB2-crystallin structure and stability. Our results implies that the oxidation of W59 unstabilizes βB2-crystallin, leading to lens dysfunction and cataract formation. This also may impact on subunit-subunit interaction among lens crystallins, result in inhibiting formation of normal-lens protein complexes [2].

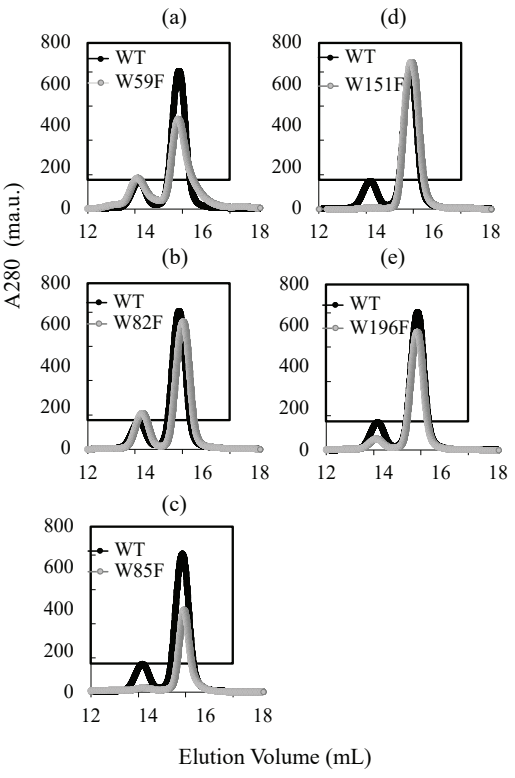

Fig. 1. Size exclusion chromatograms of βB2 mimics. WT are in black solid lines, mimics are in grey lines respectively. (a)(b)(c)(e) W59F, W82F, W85F, W196 all showed both those dimer and tetramer. (d) Only W151F only showed the dimeric peak.

REFERENCES:

[1] B. Searle *et al.,* J Proteome Res., **4** (2005) 546-554.
[2] A. Rolland *et al.,* Structure., **31** (2023) 1052–1064.

CO6-10

Spectroscopic Analysis of Tumor Model Dried Tissue in Sub-THz Region

Norio Miyoshi[1], Hidetoshi Sato[2], Bibin B. Andriana[2], and Toshiharu Takahashi[3]

[1]*Department of Cellular Immunology, Graduate School of Medical Sciences, Nagasaki University.*
[2]*Department of Life Sciences, Graduate School of Life Environment, Kwansei-Gakuin University.*
[3] *Institute for Integrated Radiation and Nuclear Science, Kyoto University*

INTRODUCTION: Spectroscopic analysis in sub-THz region in tumor pathology field is of interest in viewpoint of water interactions and important for the hydro bonding in viewpoint of MRI.

EXPERIMENTS: The experiment was performed with KURNS-LINAC. The energy of the electron beam was 39 MeV and the peak beam current measured by CT was 1.9 A. The repetition rate of the macro pulse was 60 pulses/s. Coherent transition radiation (CTR) from a titanium window was guided to the Fourier transform interferometer in the experimental room through the coherent radiation beam line [1]. A liquid-helium cooled silicon bolometer was used as the detector of CTR. The sample was prepared as tahe tumor model by cancer drug in Kwansei-Gakuin university. The sample tissue was sandwiched with two sheets of PVC plate 0.5mm thick as shown in Fig. 1.

RESULTS: As shown in Fig. 2, the spectra of tumor tissue (circle) and normal one (square) were measured. The result is shown on Fig. 3. The spectra have structure by the interference inside the PVC plate superimposed on it. Figure 4 shows the transmittivity calculated from the observed spectra. The absorption appeared in the tumor area compared with the normal one.

REFERENCES:

[1] T. Takahashi *et al.,* Rev. Sci. Instrum., **69** (1998) 3770.

Fig. 1 Experimental setup of the sample.

Fig. 2 Measurement points of tumor tissue (circle) and normal one (square).

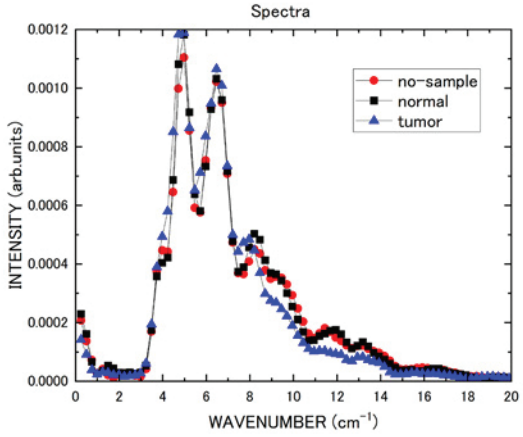

Fig. 1 The observed spectra.

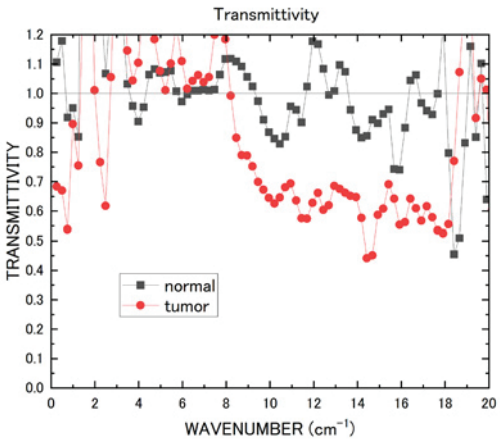

Fig. 2 The transmittivity spectra.

CO6-11

Elucidating the Molecular Basis for the Increased Risk of Nuclear Cataract Development with Global Warming

N. Yamamoto[1] and T. Takata[2]

[1] *Fujita Health University*
[2] *Institute for Integrated Radiation and Nuclear Science, Kyoto University*

INTRODUCTION: The transparency of the lens is important for focusing target onto retina. Lens cells contain rich stable long-lived structural proteins, which is called as crystallin. Recently, the worldwide epidemiological survey confirmed that the risk of nuclear cataract (NUC) is significantly higher in residents living in areas where the annual number of days with temperatures of 30°C or higher is higher. Furthermore, in an in silico simulation study, the applicant group showed that the incidence of NUC differs within a range of internal temperature differences (35.0-37.5°C) [1]. Based on these results, this study aims to clarify the relationship between the formation of NUC and temperature. There were also significant changes in cell proliferation and expression of crystallins during the process, indicating that temperature-dependent changes occur during protein biosynthesis inside the cell. After reviewing these results, we came to the hypothesis that there is a temperature dependence in the crystallin folding pathways inside the cell, and decided to conduct the following study to demonstrate temperature dependent different folding pathway in vitro.

EXPERIMENTS: Last year, recombinantly expressed human βB2-crystallin was unfolded, then refolded by dilution in the presence of each concentration of urea. The ratio of fluorescence intensities between folded (320 nm) and unfolded (360 nm) states were used for the folding index under at two different temperature environment (35.0°C vs 37.5°C). There were no differences of folding pathway between 35.0°C and 37.5°C. We, therefore, decided to create two mimics that are expected to have low thermal stability and have been reported to cause congenital cataracts [2]. Followed by previous reports, each of two tryptophan residues (Trp: W) were altered to cysteines (Cys: C) and recombinantly expressed in E.coli. at various conditions.

RESULTS: The recombinant human βB2-crystallin W59C and W151C were not well expressed in conventional vector (pET-28a vector) and BL21(DE3)pLysS cells. Therefore, we constructed his-tag and sumo tag (pET-sumo-vector) for both proteins to be expressed under mild condition and purify by Ni-column. As a result, a sufficient amount of target proteins were expressed and purified during the initial Ni-column purification (Fig. 1). However, after enzymatic treatment to cleave the his-tag and sumo, the majority was found to be lost during the second stage of purification. We think that the purification process should be further reviewed (e.g., lower temperature expression, shorter enzymatic digestion time, or use of a reducing reagents) for making those heat unstable βB2-crystallin mimics.

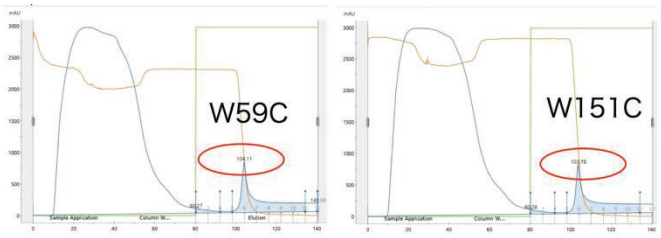

Fig. 1. Results from the first nickel column purification of βB2-crystallin mimics. Both enough amount of W59C and W151C bound to columns under current conditions.

REFERENCES:

[1] N. Yamamoto *et al.,* Cells., **12** (2020) 2670.
[2] W. Zhao *et al.,* J Biol Macromol., **103** (2017) 764–770.

CO6-12

Structural analysis of ferritin in a polyplacophoran

M. Nemoto[1], M. Shimizu[2]

[1]*Graduate School of Environmental, Life, Natural Science and Technology (Faculty of Agriculture), Okayama University*

[2]*Institute for Integrated Radiation and Nuclear Science, Kyoto University*

INTRODUCTION: Polyplacophora, a kind of mollusk, has a feeding organ called radula, in which magnetite precipitates in the cusp. Understanding the mechanism of magnetite formation by polyplacophora could lead to an environmentally friendly method for synthesizing magnetite. Since magnetite is usually produced industrially at high temperatures and with harmful substances, biosynthesis-based magnetite production will have a significant impact on the field of materials science. We have discovered a novel iron-storage protein from radula of *Acanthopleura japonica* , a species of *Polyplacophora* . To elucidate function and availability of this protein, we performed analytical ultracentrifuge and small-angle X-ray scattering on this iron-storage protein.
****

EXPERIMENTS: Analytical ultracentrifugation was performed at 40,000 rpm using a ProteomeLab XL-I analytical-ultracentrifuge (Beckman Coulter). Distribution of sedimentation coefficient was calculated by SEDFIT [1]. Small-angle X-ray scattering was performed using NANOPIX (Rigaku). One-dimension scattering profile was obtained by SAngler software [2].
****

RESULTS: Small-angle X-ray scattering data showed a characteristic profile of ferritin. Thus, this protein was suggested to have the structure of a typical ferritin protein. Ultracentrifugal analysis of this protein showed single peak in the sedimentation coefficient, and its corresponding molecular weight was around 580 kDa. Its value was almost similar to that of the protein 24-mer. These results suggest that this protein forms a typical ferritin 24-mer in aqueous solution.
****

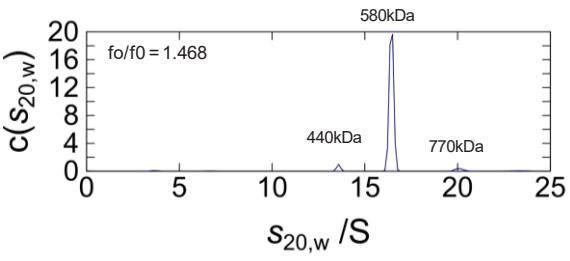

Figure 1. Sedimentation coefficient distribution of the protein

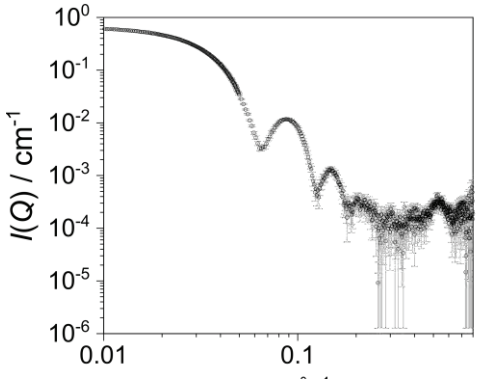

Figure 2. Small-angle X-ray scattering profile of the iron storage protein

REFERENCES:

[1] P. Schuck, Biophys. J., **78** (2000) 1606-1619.
[2] Shimizu, N. *et al.,* AIP Conf. Proc., **1741** (2016) 050017.

CO6-13

Asp racemization/isomerization in shedding products of cell adhesion molecule 1 is potentially involved in the neurodegeneration induced by elevated pressure

A. Yoneshige[1], A. Ito[1] and T. Takata[2]

[1]Department of Pathology, Kindai University
[2]Institute for Integrated Radiation and Nuclear Science, Kyoto University

INTRODUCTION: The elevation of internal pressure is often involved in neurodegeneration; intraocular and intraventricular pressure elevations over 20–30 cm H_2O cause glaucoma and hydrocephalus, respectively. Previously, to investigate the mechanisms by which elevation of intraluminal pressure causes cell or tissue de-generation, we devised a novel two-chamber culture system that enabled us to subject cultured cells to low levels of water pressure (2-50 cm H_2O pressure load) [1,2]. We found that mouse primary neurons degenerated when the water pressure was above 30 cm H_2O, and that ectodomain shedding of synaptic cell adhesion molecule 1 (CADM1) increased in a water pressure-dependent manner [1]. We also discovered that the increase of intracellular product of CADM1 shedding (C-terminal fragment, CADM1-CTF) resulted in decreased neurite density with punctate localization of CADM1 suggesting its aggregation in neurites [1]. CADM1-CTF is rich in Asp residues neighbored by Ala residues, and the conversion of these amino acids to poly-Gly diminished its aggregation state. Since the racemization and isomerization of Asp residues contributes to aggregation of various proteins and it likely occurred when the neighboring residues are small [3,4], these in-sights led us to hypothesize an involvement of Asp racemization/isomerization in the neurodegeneration induced by internal pressure elevation.
EXPERIMENTS: (1) Synthetic peptide of internal sequence of CADM1-CTF (GADDAADADTAIINAEGGQNNSEEK) was incubated at 50℃ for 0-15 days and applied to LC-MS to identify Asp isomer-containing peptides. (2) Mouse neuroblastoma cell line Neuro-2a cells with exogenously expressed CADM1-CTF were cultured un-der 50 cm H_2O and were prepared for LC-MS analysis. (3) To mimic oxidative stress induced by internal pressure elevation, Neuro-2a cells expressing CADM1-CTF were treated with hydrogen peroxide and the cells were subjected to the isolation of CADM1-CTF by immuno-precipitation (IP). The amounts and purity of CADM1-CTF-IP were quantified using immunoblotting and silver staining.
RESULTS: (1) In LC-MS analysis of CADM1-CTF synthetic pep-tide, multiple peaks were detected after 1 day at pH 6.0 or pH 7.0 indicating that Asp racemization/isomerization could occurred under neutral pH. (2) CADM1-CTF proteins in Neuro-2a cells were solubilized with water, Triton X-100 containing buffer, or SDS containing buffer after 3 days culture under 50 cm H_2O, and CADM1 immunoblot was carried out. CADM1-CTF protein yields (CADM1-CTF / total proteins) were in the order Triton X-100 > SDS > water, however, the peptide peak was not identified using with LC-MS. (3) Previously, we found that CADM1 shedding was increased by oxidative stress as a cause of pulmonary emphysema in cigarette smoke exposure [5]. We furthermore showed that Lipocalin-2, an iron binding protein was upregulated in the retinae under 50 cm H_2O pressure [6]. Since iron dysregulation induces oxidative stress, we decided to explore the linkage between oxidative stress and Asp racemization/isomerization of CADM1-CTF. We obtained partial purified CADM1-CTF from large-scale Neuro-2a cell culture, coupled with IP purification. However, the identification of Asp isomer by LC-MS remains challenging, probably because of sample purity.
REFERENCES: [1] A. Yoneshige *et al.,* Mol. Neurobiol., **54** (2017) 6378-6390. [2] M. Hagiyama *et al.,* Front. Physiol., **8** (2017) 997. [3] N. Fujii *et al.,* J. Biochem., **116** (1994) 663-669. [4] T. Takata *et al.,* Protein Sci., **29** (2020) 955-965. [5] A. Ri *et al.,* Front. Cell Dev. Biol., **6** (2018) 52. [6] A. Yoneshige *et al.,* Front. Cell Dev. Biol., **9** (2021) 664327.

CO6-14

Small-angle X-ray scattering analysis of MDP1-DNA mixture

M. Shimizu

Institute for Integrated Radiation and Nuclear Science, Kyoto University

INTRODUCTION: MDP1 is a protein of Mycobacterium sp. that is involved in intracellular Fe ion dynamics [1]. At the same time, the protein binds to nucleic acids and functions to bundle them [2]. To further elucidate the structure and function of MDP1, we analyzed the structure of mixed state of peptide whose sequence is characteristic of MDP1 and DNA by small-angle X-ray scattering measurements.

EXPERIMENTS: Peptide and DNA were purchased from Eurofins Genomics. Both peptide and DNA were dissolved in D_2O. Small-angle X-ray scattering was performed using NANOPIX (Rigaku). One-dimension scattering profile was obtained by SAngler software [3].

RESULTS: Radius of gyration (R_g) was calculated for the mixture system. The R_g was 18.7 Å. On the other hand, the R_g for DNA alone was 16.9 Å. Thus, DNA and peptides were shown to form a complex. We note that the detailed size distribution of the complex cannot be determined from the scattering profile alone. Considering that the molecular weight of the peptide alone is around 2,000 Da, there can be a mixture of free peptide and a much larger complex. This peptide is strongly positively charged and has been reported in the past to interact strongly with DNA [4]. This experiment showed consistency with the present experiment. On the other hand, no other characteristic scattering profiles appeared by mixing. In other words, the mixing of peptide and DNA did not dictate the formation of a new regular structure.

REFERENCES:

[1] S. D. Pandey *et al.,* J. Bacteriol., **196** (2014) 1853-1865.

[2] A. Nishiyama *et al.,* Nucleic Acid Res., **52** (2024) 816-830.

[3] N. Shimizu *et al.,* AIP Conf. Proc., **1741** (2016) 050017.

[4] M. Furugen *et al.,* Microbial Pathogenesis, **30** (2001) 129-138.

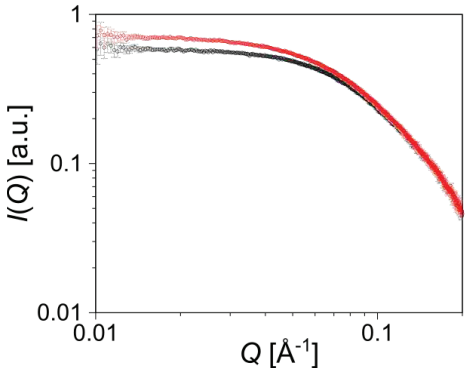

Figure 1. Small-angle X-ray scattering profile of the mixture of DNA and MDP1 peptide (red) and DNA (black).

CO6-15

Effect of salt concentration on solution structure of intrinsically disordered protein

R. Inoue, T. Oda[1], and M. Sugiyama

Institute for Integrated Radiation and Nuclear Science, Kyoto University
[1]J-PARC Center, JAEA

INTRODUCTION: Compared to the solution structure of folded globular protein (FDP), the solution structure of intrinsically disordered protein (IDP) exhibits a different susceptibility against external environment dependence due to the high content of hydrophilic and polar residues. For example, radius gyration (R_g) increases with increasing temperature for FDP, on the other hand it decreases with increasing temperature for IDP [1]. It is considered that enhancement of hydropho-bic interaction at high temperature could be concerned for such anomalous temperature-dependent structural change observed for IDP, however direct experimental proof for such an expectation have not obtained yet. In this work, we investigated the solution of IDP at two different salt concentra-tions and discussed whether or not enhancement of hydrophobic interaction at high temperature is the main contributor for the anomalous temperature-dependent structural change of IDP

EXPERIMENTS: As an example of IDP, we used intrinsically disordered region of Hef (Hef-IDR) [2]. To examine the solution of structure of Hef-IDR, we performed small-angle X-ray scattering (SAXS) measurements. SAXS measurements were conducted using a Photon Factory BL-6A instrument (Tsukuba, Japan). The X-ray wavelength and the sample-to-camera distance were set to 1.5 Å and 2038.9 mm, respectively. The Hef-IDR solution at the concentration of 12 mg/mL was prepared in a buffer containing 10 mM Tris (2-carboxyethyl) phosphine hydrochloride and TCEP (10 mM HEPES pH 7.5, 100 mM NaCl, 0.1 mM EDTA, 10 mM TCEP).

RESULTS: Fig. 1 shows the temperature dependence of R_g at two different salt concentrations. It is evident that R_g value is not affected by change of salt concentration, denying the possibility that decrease of R_g with increasing temperature is not caused by the enhancement of hydrophobic interaction at high temperature. From the complementary uses of various techniques, it was revealed that loss of polyproline type II helix at high temperature was mainly responsible for the decrease of R_g at high temperature observed for Hef-IDR [3]. At present, we are planning to perform SAXS measurement of Hef-IDR at different external environment such as high pressure.

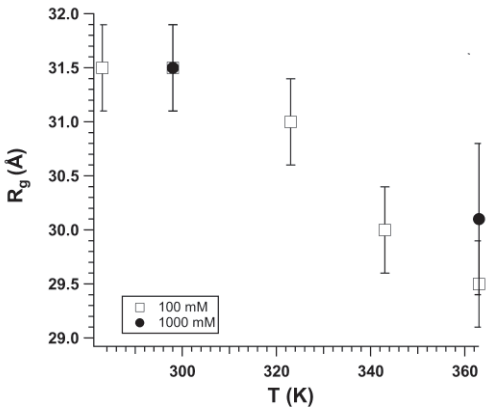

Fig. 1. Temperature dependence of R_g of Hef-IDR at 100 mM and 1000 mM.

REFERENCES:

[1] V. N. Uversky, J.R. Gillespie, and A.L. Fink. Pro-teins, **41** (2000) 415–427.
[2] S. Ishino *et al.,* J. Biol. Chem., **289** (2014) 21627-21639.
[3] R. Inoue *et al.,* Biophys. J., **124** (2025) 540-548.

CO6-16

Complex formation of cyanobacterial circadian clock proteins in solution

K. Morishima, R. Sakamoto, M. Shimizu, R. Inoue, and M. Sugiyama

Institute for Integrated Radiation and Nuclear Science, Kyoto University

INTRODUCTION:

Cyanobacterial circadian clock is composed of three clock proteins, KaiA, KaiB and KaiC, and its circadian rhythm is observed as a 24-hour cycle of the degree of phosphorylation of KaiC. The phosphorylation of KaiC is promoted by the formation of the KaiA-KaiC complex, and conversely, it is dephosphorylated by the formation of the KaiB-KaiC complex. In other words, to understand the oscillation mechanism of the circadian rhythm, it is essential to elucidate the competitive complex formation behaviour of KaiA and KaiB towards KaiC. In the previous research, we have clarified the phosphorylation state dependence of the KaiA-KaiC complex. Then, in this study, we focus on the KaiB-KaiC complexes formation utilizing phosphorylation-mimicking KaiC mutants

EXPERIMENTS:

Analytical ultracentrifugation (AUC) measurements was performed for titration samples of KaiB+KaiC. To mimicking the phosphorylation states of KaiC, we used the following mutants: S/T–mimicking S431A/T432A mutant ($KaiC_{AA}$), S/pT–mimicking S431A/T432E mutant ($KaiC_{AE}$), pS/pT–mimicking S431D/T432E mutant ($KaiC_{DE}$), and pS/T–mimicking S431D/T432A mutant ($KaiC_{DA}$). KaiB+KaiC titration sample series was prepared by mixing KaiB and KaiC solutions with the composition of [KaiB] : [KaiC] = x : 6 (x = 0 – 12), where [KaiB] and [KaiC] mean the molar concentration for their monomer. The partial concentration of KaiC was fixed at 2.0 mg/mL. The solution was subjected to measurements after incubation at 30 °C for 24 hours. AUC measurements were performed using ProteomeLab XL-I (Beckman Coulte). Sedimentation velocity analysis was performed using Rayleigh interference optics at 30 °C. The rotor speed was set at 60,000 rpm. The weight-concentration distributions as a function of sedimentation coefficient $c(s_{20,w})$ and average frictional ratio f/f_0 were obtained through computational fitting to the time evolution sedimentation data with the multi-component Lamm formula using SEDFIT software version 15.01c [1]

RESULTS:

Fig1(a) show the titration-AUC result for the mix solution of KaiB+ $KaiC_{DE}$. With the KaiB mixing ratio increased, the peak shifted continuously to the higher $s_{20,w}$ side, and converged at $s_{20,w}$ = 12.3 S which corresponds to B_6C_6. Fig1(b) show the KaiC-phosphorylation dependence of the B_6C_6 formation. It is very noteworthy that, other than $KaiC_{DE}$, the phosphorylation mimics do not form B_6C_6. This means that the ability to form BC complexes is dramatically different between the highly phosphorylated state (DE) and other states. This phosphorylation-state-dependent affinity is one of the principles that generates the circadian oscillation of this system.

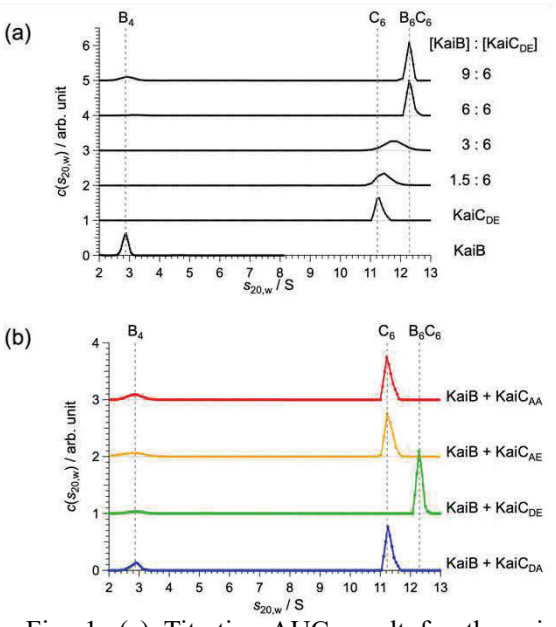

Fig. 1. (a) Titration-AUC result for the mix solution of KaiB+ $KaiC_{DE}$ with various mixing ratios. (b) AUC results for the mix solution of KaiB+ $KaiC_{DE}$ at the mixing ratio of [KaiB] : [KaiC] = 7.5 : 6 for various KaiC mutants.

REFERENCES:

[1] P. Schuck, Biophys, J., **78** (2000) 1606-1619.

CO6-17

Character of DNA damage induced by nuclear plant neutron beams

H. Terato, T. Hanafusa[1], M. Isobe, Y. Sakurai[2], H. Tanaka[2], and T. Saito[2]

Advanced Science Research Center, Okayama University
[1]Neutron Therapy Research Center, Okayama University
[2]Institute for Integrated Radiation and Nuclear Science, Kyoto University

INTRODUCTION: Radiation-induced biological effects are expressed through damage to DNA. Therefore, analyzing radiation-induced DNA damage is essential for elucidating the molecular mechanisms underlying these biological effects. High-LET radiation, such as heavy ion beams and neutron radiation, induces types of DNA damage that differ from those caused by low-LET radiation like gamma-rays [1, 2]. Two specific forms of DNA damage associated with high-LET radiation are cross-linked DNA damage (CLD) and clustered DNA damage (CDD). These types of damage show strong inhibitory effects on DNA synthesis and their low repair efficiency [3–5]. In this study, we aimed to analyze DNA damage caused by reactor neutrons, the two types of damage, CLD and CDD, also play a significant role in the expression of neutron-specific biological effects. Furthermore, we also analyzed the forms of DNA damage associated with Boron Neutron Capture Therapy (BNCT), a medical application of neutron radiation.

EXPERIMENTS: pUC19 DNA was dissolved in TE buffer (10 mM Tris-HCl, pH 7.5, 1 mM ethylenediaminetetraacetic acid) containing 1 M dimethyl sulfoxide and dispensed into microtubes. Samples with and without BSH (^{10}B-sodium mercaptododecaborate), one of BNCT agent, were prepared, and neutron irradiation was carried out at the KUR. The BSH concentration was set to 10% (w/v). Radiation doses were up to 5 Gy as a total physical dose. After irradiation, DNA was dialyzed against TE buffer to remove BSH, separated using 0.8% agarose gel electrophoresis, and the generated DNA damage was analyzed [1, 2].

RESULTS: The DNA damage in pUC19 was assessed using neutral agarose gel electrophoresis, which allows the separation of the circular plasmid DNA into three forms: type I (undamaged circular DNA), type II (single-strand break, SSB), and type III (double-strand break, DSB), thus enabling the observation of SSBs and DSBs in the DNA [1]. The results of agarose gel electrophoresis of irradiated DNA showed that DNA damage increased in a dose-dependent manner. The damage-enhancing effect of BSH was particularly prominent at low-dose regions, with a maximum increase in damage of up to fivefold. Most of the DNA damage detected by agarose gel electrophoresis was DSBs rather than SSBs. This suggests that high-LET radiation including neutrons and alpha particles with BNCT, efficiently induces DSBs. DSB is one of CDD induced by ionizing radiation directly and indirectly. In future studies, we plan to investigate another BNCT drug, BPA (^{10}B-4-Borono-L-phenylalanine), to further clarify the effects of BNCT.

REFERENCES:
[1] H. Terato *et al.*, J. Radiat. Res., **49** (2008) 133-146.
[2] Y. Tokuyama *et al.,* J. Radiat. Res., **56** (2015) 446-455.
[3] Y. Kinashi *et al.,* Radiat. Oncol., **6** (2011) 106.
[4] H. Terato *et al.,* KURNS Progress report 2022, (2023) 158.
[5] T. Nakano *et al.,* J. Biol. Chem., **284** (2009) 27065-27076.

CO6-18

Small-angle X-ray scattering analysis of di-nucleosomes

S. Sato[1], K. Morishima[2], R. Inoue[2], A. Okuda[2], M. Dacher[1], N. Horikoshi[1], M. Sugiyama[2], H. Kurumizaka[1]

[1]*Institute for Quantitative Biosciences, The University of Tokyo*
[2]*Institute for Integrated Radiation and Nuclear Science, Kyoto University*

INTRODUCTION: In eukaryotes, including human pathogenic parasites, genomic DNA forms chromatin structure and is packed within the nucleus. Chromatin plays an essential role in regulating biological events such as gene transcription, DNA repair, and replication by dynamically changing its conformation. The conformation of chromatin, in terms of compaction and relaxing forms, is regulated by histone modifications and binding proteins. Chromatin is an array of nucleosomes, each composed of 145-147 base-pairs of DNA wrapped around a histone octamer containing two molecules each of histone proteins H2A, H2B, H3, and H4. The relative positioning and flexibility between nucleosomes are important for chromatin conformation. Therefore, we tried to establish a method for analyzing the structures of adjacent nucleosomes in solution. We used di-nucleosomes in which two nucleosomes are connected by a linker DNA, and applied small-angle X-ray scattering (SAXS). This approach is important for understanding the mechanisms of chromatin dynamics regulated by epigenetic factors in eukaryotic cells.

EXPERIMENTS: Di-nucleosomes were prepared by in vitro reconstitution [1]. Recombinant histones were mixed with a DNA fragment under high salt conditions, followed by a gradual decrease in salt concentration to promote nucleosome formation. Di-nucleosomes were then purified using a method based on polyacrylamide gel electrophoresis [1]. The di-nucleosomes thus obtained were analyzed by SAXS. SAXS intensity of the buffer solution was measured for background subtraction, using the same procedure as for the di-nucleosome samples. These SAXS data were collected using a laboratory-based instrument equipped with a high-brilliance point-focused generator of a Cu Kα source. To assess aggregation and dissociation of the sample, sedimentation velocity was measured by analytical ultracentrifugation (AUC) [2].

RESULTS: We confirmed the formation of di-nucleosomes on the DNA fragment containing two strong nucleosome positioning sequences with 15-base pairs of linker DNA by polyacrylamide gel electrophoresis. We carefully removed precipitates by centrifugation and the di-nucleosome solution was prepared at a sufficient concentration for SAXS analysis. The AUC results showed a major peak corresponding to the di-nucleosome, and a small amount of dissociated and aggregated components were detected. Scattering profile (one-dimensional intensity data I(q) as a function of (q)) of the di-nucleosome was calculated as aggregated components were removed. Radius of gyrations (R_g) were estimated from the fitting curves of the I(q) data using Guinier plot, as previously described [3]. This analysis will be further pursued to establish a method for observing chromatin compaction in solution.

REFERENCES:

[1] T. Kujirai *et al.,* Methods Mol. Biol., **1832** (2018) 3-20.
[2] K. Morishima *et al.,* J. Appl. Crystallogr., **56** (2023) 56, 624-632.
[3] Y. Arimura *et al.,* Sci. Rep., (2013) 3510.

CO6-19

Design, Synthesis, and Evaluation of Macrocyclic Polyamine-Based Multiboron Carriers for BNCT

S. Aoki[1,2], H. Ueda[3], W. Yoshida[1], M. Suzuki[3], Tanaka, T.[1,4] S Masunaga[3], N. Kondo[3], and Y. Sakurai[3]

[1]*Faculty of Pharmaceutical Sciences, Tokyo University of Science*
[2]*Research Institute for Science and Technology, Tokyo University of Science*
[3]*Research Reactor Institute, Kyoto University*
[4]*Faculty of Pharmaceutical Sciences, Okayama University*

INTRODUCTION: Neutron capture therapy using boron-10 (^{10}B) (BNCT) is one of powerful therapies for local tumor control in the treatment of brain tumor, melanoma, and related diseases. We previously designed and synthesized phenylboronic acid-pendant 9-, 12-, and 15-membered macrocyclic amines such as **^{10}B-1a~3a** and the corresponding Zn^{2+} complexes **^{10}B-1b~3b** (Fig. 1) [1,2], based on high intracellular uptake of cyclen (1,4,7,10-tetraazacyclododecane) derivatives in cancer cells. It was reported that the metal-free **^{10}B-1a~3a** are introduced into cancer cells (A549 and HeLa S3 cells) more efficiently than their Zn^{2+} complexes **^{10}B-1b~3b** with considerably high cancer/normal cells selectivity. Besides, it was found that 12- and 15-membered derivatives **^{10}B-2a~3a** exhibit a higher BNCT effect than **^{10}B-1a**, possibly because **^{10}B-2a~3a** form the corresponding Zn^{2+} complexes **^{10}B-2b** & **3b**, which strongly interact with DNA in living cells [3], resulting in the efficient breakdown of DNA upon the neutron irradiation.

Next, we synthesized dimeric macrocyclic polyamines having one phenylboronic acid unit such as **4~9** and their corresponding Zn^{2+} complexes (Fig. 1), because it was well established that polymeric Zn^{2+} complexes would form more stable complexes with DNA double strand than monomeric Zn^{2+} complexes [4]. However, the intracellular uptake of **4~9** and their Zn^{2+} complexes were lower than monomeric compounds **1~3**, possibly due to their lower hydrophobicity than that of **1~3.**

EXPERIMENTS AND RESULTS:

The aforementioned results have prompted us to synthesize monomeric polyamines equipped with two boronic ester units for higher intracellular uptake and BNCT effect. In 2024, **10a~15a** and their corresponding Zn^{2+} complexes **10b~15b** (Fig. 1) were synthesized. The evaluation of intracellular uptake and BNCT effect of **10a~15a** and **10b~15b** has suggested that **14a** has highest intracellular uptake and BNCT effect among these compounds [5].

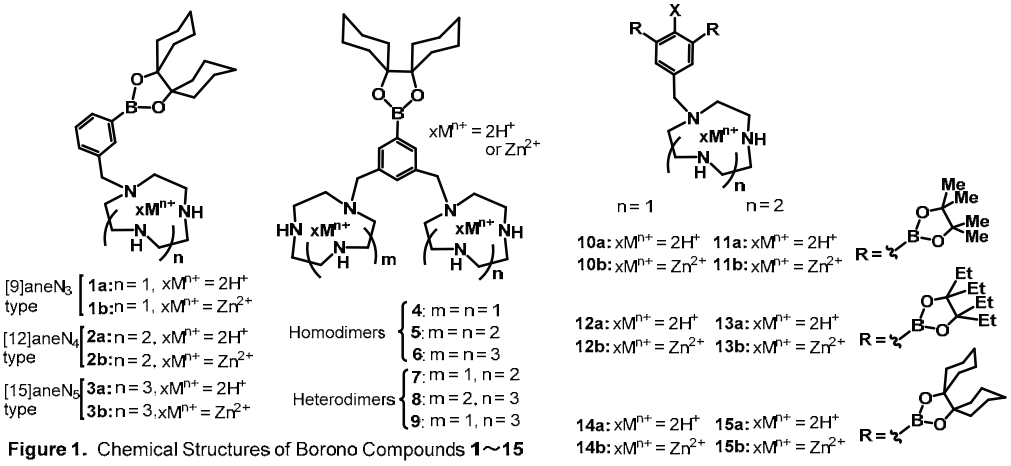

Figure 1. Chemical Structures of Borono Compounds **1~15**

REFERENCES:

[1] H. Ueda *et al.,* J. Med. Chem., **64** (2021) 8523-8544.
[2] S. Aoki *et al.,* In "*Characteristics and Applications of Boron*" 2022, pp 83-105, Charchawal Wongchoosuk, Ed., IntechOpen, Croatia.
[3] S. Aoki *et al.,* Chem. Rev., **104** (2004) 769-788.
[4] H. Ueda *et al.,* Eur. J. Inorg. Chem., **2022** (2022) e202100949 (24 pages).
[5] W. Yoshida *et al.,* Manuscript in preparation.

CO6-20

Quantitative change on microglia and astrocytes in the brain after immuno- and/or radiation therapy for cancer

Natsuko Kondo[1], Yoichi Shimizu[2], Nao Kobayashi[2] and Yoshinori Sakurai[1]

[1] Particle Radiation Oncology Research Center, Institute for Integrated Radiation and Nuclear Science, Kyoto University (KURNS)
[2]Dept. of Diagnostic Imaging and Nuclear Medicine, Graduate School of Medicine, Kyoto University.

INTRODUCTION: Radiotherapy such as X-rays and γ-rays is used as a standard treatment as a safe and effective cancer treatment. There are many unknown points, such as the interaction between infiltrated immune cells and residual tumors in the microenvironment, the effects of immune cells on organs and tumors outside the irradiated area. In addition, immune checkpoint inhibitors have come into use, and interactions mediated by immune cells have been emphasized. In this study, we investigated how immune cells infiltrate and interact with irradiated tissues and organs throughout the body (outside the field of irradiation), including the brain, after irradiation. We will also investigate the changes that occur when immune checkpoint inhibitors are used in combination with radiation therapy.

EXPERIMENTS:

Cells:

We used Lewis Lung Cell Carcinoma cell line (LLC). They were cultured in RPMI 1640 medium with 10% heat-inactivated fetal bovine serum in 5 % CO_2 incubator.

Innoculation of tumor and drug treatment to animals

We used C57BL/6 mice. $5E^5$ LLC cells were inoculated subcutaneously in a thigh of the mice. We created four groups (non-treatment, immunotherapy alone, radiation therapy alone, and immunotherapy and radiation therapy combined) and each group contained 9 animals. After the inoculation, we administrated anti-mouse PD-1 antibody on the day 6 and 12 (250 μg/body).

Irradiation:

We used the Cobalt 60 gamma-ray irradiation device in KURNS. On the day 13, we irradiated the tumor on the thigh of mice at the dose of 20 Gy shielding the body and head with lead.

Measurement of tumor size and sampling of tumors and brains

After the irradiation, we measured the major and minor axes of the tumors until mice were sacrificed. We sacrificed three mice in each group on 2, 7, 14 days after irradiation. The brain and tumor were removed and fixed in 10 % buffered formalin for pathological samples.

Immunohistochemistry:

We prepared paraffin sections, and stained microglia or macrophages using a monoclonal Iba-1 antibody for 1st antibody. DAB staining was used for second antibody. We analyzed the numbers of Iba-1 or GFAP positive cells in the hippocampus and cortex of the brain or in the tumor.

Mouse behavioral analysis

We performed the behavioral analysis with the mice after drug-treatment and/or irradiation.

RESULTS:

Tumor size: Only in the combination group, tumor size was significantly reduced compared with the control at 14 days after irradiation.

Pathology: The number of microglia in hippocampus tended to increase in immunotherapy alone group at 2 and 7 days after irradiation. In the tumor, the macrophages increased 7 days after irradiation.

Mouse behavioral analysis

Currently we are conducting mouse behavior analysis.

CO6-21

^{11}C Medical-isotope Production via ^{12}C(γ,n)^{11}C Reaction with Single-walled Carbon Nanotubes

N. Takahashi[1,2], M. Kurosawa[1], M. Tamura[1], M. Fujiwara[1,2], T. Kubota[3], N. Abe[4], and T. Takahashi[4]

[1]Research Center for Nuclear Physics, Osaka University
[2]Kyoto Medical Technology
[3]Agency for Health, Safety and Environment, Kyoto University
[4]Institute for Integrated Radiation and Nuclear Science, Kyoto University

INTRODUCTION: L-[^{11}C]-Methionine is used as a positron emission tomography (PET) reagent for medical diagnosis of brain tumors [1]. The medical ^{11}C radioisotopes are mostly produced in a cyclotron via the ^{14}N(p,α)^{11}C reaction by bombarding enriched nitrogen gas with a proton beam [2]. Instead of producing ^{11}C with the cyclotron, we developed a novel method of producing ^{11}C using the bremsstrahlung γ-rays with a single-walled carbon nanotubes (SWCNT) to get a reasona-ble number of the ^{11}C activity.

EXPERIMENTS: Figure 1 shows the experimental scheme for the ^{11}C production via the ^{12}C(γ,n)^{11}C reaction. Bremsstrahlung γ-rays were produced by impinging a 40 MeV electron beam on platinum converter at the electron LINAC facility. The γ-rays were irradiated to SWCNT sealed in aluminum vessel with non-woven masks as gas inlet/outlet filter. The produced ^{11}C inside the vessel were oxidized to ^{11}CO or ^{11}CO$_2$ in O$_2$ gas, which was continuously flown during the irradiation. The ^{11}C gas (^{11}CO and ^{11}CO$_2$) were trapped in two 13X molecular sieve columns and 511-keV γ-rays from positron-electron annihilation were detected with CdZnTe detectors. The SWCNT with a diameter of 2-3 nm were used as target.

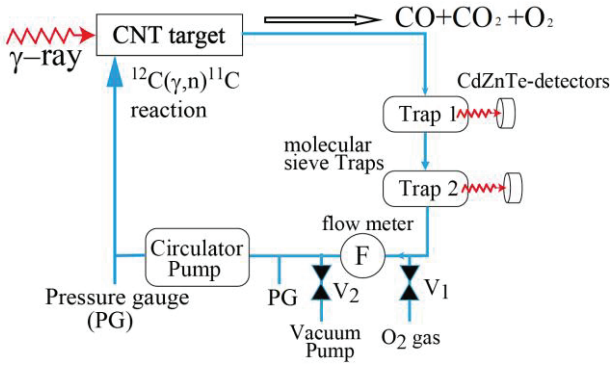

Fig. 1 Experimental scheme to produce ^{11}C and measure the extraction rate of ^{11}C gas.

RESULTS: Table 1 shows the normalized activity of ^{11}C gas for SWCNT which have different bulk density. The normalized activity slightly increases as bulk density increased. All the values shown in Table 1 are higher than 8.71 kBq/μA/g/min for SWCNT with a diameter of 1-1.4 nm used in the previous experiments.

Based on the experimental production rate of ^{11}C gas, we estimate that we can obtain the ^{11}C activity of 58 GBq when we use a SWCNT target under the conditions with 1) a length of 50 cm, 2) weight of 1.13 kg for 0.155 g/cm^3, 3) a 40 MeV electron beam intensity of 100 μA for 40 minutes bombardment.

Table 1 Normalized activity of ^{11}C gas for each bulk density

Bulk density of SWCNT (mg/cm^3)	Normalized activity of ^{11}C gas (kBq/μA/g/min)
3.27	13.30±0.07
6.53	13.94±0.07
9.80	14.41±0.06
13.06	14.92±0.05

REFERENCES:

[1] Kobayashi K. *et al.,* Eur. J. Nucl. Med. Mol. Imaging, **42** (2015) 1071-1080.
[2] David R. Christman *et al.,* Int. J. appl. radiat. isot., **26** (1975) 435-442.

CO6-22

Analysis of flexible structure of multi-domain protein Hef

T. Oda, R. Inoue[1], K. Morishima[1], A. Okuda[1], M. Sugiyama[1]

J-PARC Center, Japan Atomic Energy Agency.
[1]Institute for Integrated Radiation and Nuclear Science, Kyoto University.

INTRODUCTION: Hef is a protein that is required for DNA repair in hyperthermophilic archaea [1,2]. Hef consists of an N-terminal helicase domain, a C-terminal nuclease domain and intrinsically disordered region (IDR) connecting them [1,2]. Due to flexibility of the IDR, structural analysis of Hef using crystallography or cryo-electron microscopy is difficult. In this study, we attempted to analyze the flexible structure of Hef using small angle X-ray/neutron scattering (SAXS/SANS). Since the entire molecule contributes to scattering in SAXS, it is difficult to determine the ensemble structure of a multi-domain protein based solely on the SAXS profile. Therefore, to obtain another experimental constraint, we prepared a full-length Hef with 75% deuteration in only the helicase or the nuclease domain (segmentally deuterated samples, Fig.1(a)). If SANS measurement of the segmentally deuterated samples is performed in 100% D_2O solvent, the 75% deuterated domain is matched out, and only scattering of the non-deuterated region can be observed. Therefore, it is expected that the ensemble structure can be determined correctly by combining it with the SAXS profile.

EXPERIMENTS: Deuteration of Hef or D_2O solvent may affect the structure of Hef. In this study, prior to the SANS experiment, we performed SAXS analysis of the segmentally deuterated samples to confirm the presence or absence of structural modulation due to deuteration or D_2O solvent. The segmentally deuterated samples were prepared by ligation the 75% deuterated domain and the non-deuterated region using a protein ligation enzyme. After protein preparation, the solvent of samples was exchanged to D_2O buffer. The SAXS measurements were performed with BL10C installed PF. To avoid aggregation, SAXS measurements were carried out using dilute samples (0.6 mg/ml).

RESULTS: The SAXS profiles of the segmentally deuterated samples in D_2O and the fully hydrogenated sample in H_2O are shown in Fig1(b). The R_g values of segmentally deuterated samples (44 ±1Å and 47±2Å,) were equivalent to that of the fully hydrogenated sample (45±1Å). There was no difference between the SAXS profiles of the segmentally deuterated samples and the fully hydrogenated sample. These results show that there is no structural difference between the segmentally deuterated samples in D_2O and the fully hydrogenated sample in H_2O.

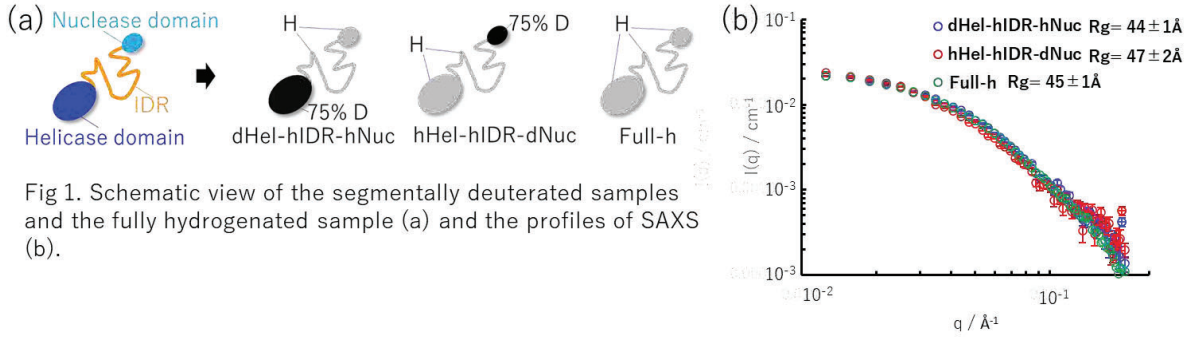

Fig 1. Schematic view of the segmentally deuterated samples and the fully hydrogenated sample (a) and the profiles of SAXS (b).

REFERENCES:

[1] Fujikane *et al.*, Genes Genet. Syst., **85** (2010) 243.
[2] Ishino *et al.*, J. Biol. Chem., **289** (2014) 21627.

CO6-23

Biophysical analysis of higher-order multimers of p53 DNA binding domain

E. Hibino[1], R. Hijikata[1], K. Morishima[2], R. Inoue[2], M. Sugiyama[2] and H. Hiroaki[1,3,4]

[1]*Graduate School of Pharmaceutical Sciences, Nagoya University*
[2]*Institute for Integrated Radiation and Nuclear Science, Kyoto University*
[3]*BeCellBar LLC.*
[4]*COMIT*

INTRODUCTION: The p53 protein functions as a crucial transcription factor for suppressing oncogenesis. Under cellular stress, p53 is activated and its expression levels rise, leading to the transcription of target genes that induce cell cycle arrest and apoptosis[1]. However, p53 can be inactivated through two distinct pathways: aggregation promoted by p53 DNA-binding domain (p53-DBD) and MDM2-mediated degradation[2]. Both mechanisms significantly contribute to tumorigenesis. Restoring functional p53, either by using p53 aggregation inhibitors or MDM2 inhibitors, has become a central approach in the development of anticancer therapies. Recently, we examined the p53 aggregation inhibitory activity of 16 flavonoids. We found that baicalein, which has been reported to exhibit some anticancer activity[3,4], suppresses aggregation of p53-DBD in vitro. In this study, we aimed to elucidate the mechanism of the anticancer effect of baicalein via p53 and analyzed the effect of baicalein on p53.

EXPERIMENTS: p53-DBD was produced using an E. coli overexpression system[5]. The purified p53-DBD solution was mixed with baicalein and incubated at 37°C for 1 h. The samples were then analyzed by Blue Native PAGE, nanoparticle tracking analysis (NTA), and dynamic light scattering (DLS), and observed by transmission electron microscopy (TEM).

RESULTS: After incubation of p53-DBD solution at 37°C for 1 h, amorphous aggregates and amyloid aggregates were formed, but it was found that the addition of baicalein suppressed these aggregate formations. Accordingly, we hypothesized that monomeric p53-DBD molecules remained, and confirmed the size of the molecules contained in the solution by Blue Native PAGE. As a result, it was suggested that p53-DBD forms relatively large particles by baicalein. Therefore, the formed particles were examined by NTA, TEM, and DLS, and it was found that higher-order multimers were formed in a concentration-dependent manner of baicalein (Fig. 1). We propose that the formation of p53-DBD higher-order multimers by baicalein leads to the inactivation of p53-DBD and maintains its function.

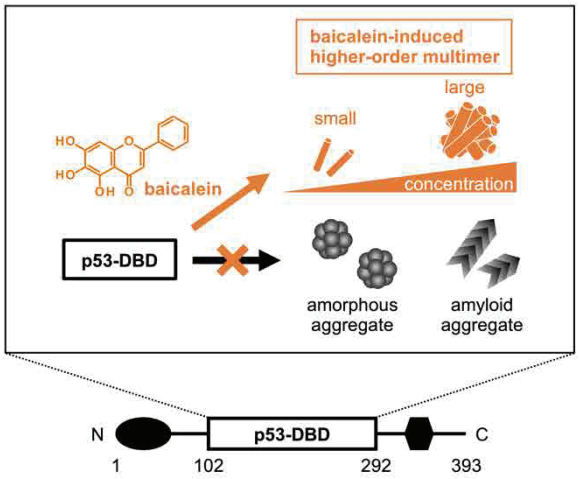

Fig. 1 Baicalein inhibits both amorphous and amyloid aggregation of p53-DBD and induces another higher-order multimer of p53-DBD in a concentration-dependent manner.

REFERENCES:

[1] B. Vogelstein *et al.,* Nature, **408** (2000) 307–310.
[2] E. Hibino *et al.,* Biophys. Rev, **14** (2022) 267–275.
[3] W. Yan *et al.,* Drug Des. Devel. Ther., **12** (2018) 3961–3972.
[4] Y. Gao *et al.,* Medicinal Chemistry Research, **25** (2016) 1515–1523.
[5] E. Hibino *et al.,* Front. Mol. Biosci., **9** (2022) 869851.

CO6-24

Distribution analysis of the chemical modification of the amino acid residues in mice lens structural proteins during age-related cataract

S. Matsushita[1], Y. Suzuki[1] and T. Takata[2]

[1] *Dept of Materials and Applied Chemistry, Nihon University*
[2] *Institute for Integrated Radiation and Nuclear Science, Kyoto University*

INTRODUCTION: Age-related cataracts are the leading causes of blindness in world. Several risk factors, contributing to the development of cataracts, have been reported. Above all, abnormal lens protein aggregation and insolubilization has been believed as the main process. Alteration of lens protein structure, caused by covalently post-translational modifications, are thought to be critical for maintaining lens protein homeostasis [1]. We have shown that covalent modifications of amino acid residues as a scale for a lens aging. To do this, mass spectrometry is an efficient tool to quantitative analysis, however the distributions of modifications were very obscured. Therefore, we are to address revealing the distribution of modifications (isomerization/racemization of Asp) in the lens section using by Imaging Mass Spectrometry (IMS) [2]. This technique requires the preparation of high-quality sections, but we could not have prepared the samples available for IMS so far. Since it has been very difficult to attach water-rich lens tissues to analytical glass plate, we tried to analyze lens model peptide with matrix solution on the sample plate to identify peptide by molar mass.

EXPERIMENTS: We synthesized, purified lens model peptides and mixed with CHCA ((4-hydroxyphenyl) acrylic Acid)), which is matrix for MALDI TOF-MS, in the presence of 50% acetonitrile. Each of modification site (L-α-Asp, L-β-Asp, D-α-Asp, D-β-Asp) were confirmed using by LC-MS/MS systems in Institute for Integrated Radiation and Nuclear Science, Kyoto University (data not shown). Then, we directly those samples with CHCA and loaded onto the imaging plate under three different concentration of peptide (Fig. 1). This is because of that to obtain subtracted MS images before digestion. The data was obtained by positive ion mode at m/z 100-2500 using by JMS-S3000 (JEOL). The peak at m/z 1311.70-1312.05 was observed (Fig. 2).

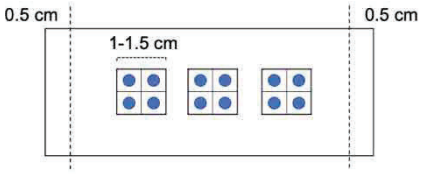

Fig. 1. The schematic drawings for added samples/CHCA mixtures into glass plate under three different concentrations.

RESULTS: The result suggested that the peptide concentration above 2.5 mg/mL show the images of peptides. The each of peptide had the same m/z, but D-α-Asp and D-β-Asp containing intense images. The mixed state with matrix and ionized state may have some differences between L-Asp or D-Asp. The shape is not simple image but heterogeneity. Drying from droplets mixing samples and matrix can form debris on the plate. To escape from this issue, the uniformed spraying system for samples/matrix should be constructed. Last year, we prepared that system and protease for D-Asp containing peptide/protein. To the end, we success to obtain the optimized samples concentrations, right m/z and specific enzyme for this study. After check the activity of this enzyme, we will use all for IMS systems.

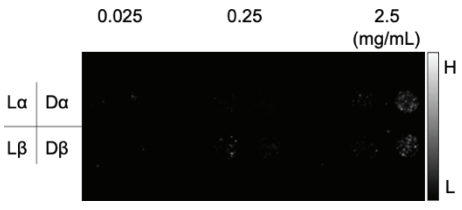

Fig. 2. The MS imaging of peptide that including *m/z* 1311.70 1312.05.

REFERENCES:

[1] N. Fujii *et al.,* Biochim. Biophys. Acta, **1860** (2016) 183-191.
[2] J. McMahon *et al.,* J. Am. Soc. Mass. Spectrrom., **11** (1995) 1047-1058.

CO6-25

Molecular dynamics analysis of oxidative folding enzyme ER-60 with solution scattering measurement

A. Okuda, M. Shimizu, K. Morishima, R. Inoue, R. Urade and M. Sugiyama

Institute for Integrated Radiation and Nuclear Science, Kyoto University

INTRODUCTION: ER-60 is a multi-domain oxidative protein folding enzyme with the domain order **a-b-b-b'-a'**. The **a** and **a'** domains contain catalytically active cysteine pairs. During oxidative protein folding, ER-60 is thought to adopt specific domain conformations essential for its function. It is also hypothesized that its overall structure dynamically fluctuates in response to the redox state of the active cysteine pairs in solution [1]. Neutron scattering is a valuable technique for investigating such structural dynamics in solutions. It exploits the large difference in neutron scattering length between hydrogen and deuterium, making it particularly useful for studying multi-domain proteins like ER-60. In a 100% deuterated solvent, 75% deuterated proteins become scatteringly invisible, allowing selective observation of hydrogenated domains in multi-domain proteins. Applying this method to multi-domain proteins, the domain of the hydrogenated domains could be selectively observed. To elucidate the structure–function relationships of ER-60, we aim to analyze individual domain structures using inverse contrast-matching small-angle neutron scattering (iCM-SANS) [2]. For this purpose, segmentally deuterated ER-60 proteins were prepared by connecting individual domains using the ligation enzyme OaAEP [3].

EXPERIMENTS: The 75% deuterated (d) and hydrogenated (h) domains were expressed in E. coli cultured in M9 medium containing 75% deuterium and LB medium without deuterium, respectively [4]. The purified domains were mixed in buffer containing 200 mM Tris-HCl (pH 7.4) / 150 mM NaCl. Then, 0.2 μM of the ligation enzyme OaAEP was added to the mixture, and the protein ligation reaction was performed at 20°C for 64 hours. The results of ligation reactions were confirmed by SDS-PAGE. SAXS measurements were performed at 25 °C with 4 hours of exposure- time using a NANOPIX (Rigaku, Tokyo, Japan). The sample-to-detector distance was set to 1330 mm and 300 mm. The q range was from 0.01 to 0.80 Å $^{-1}$.

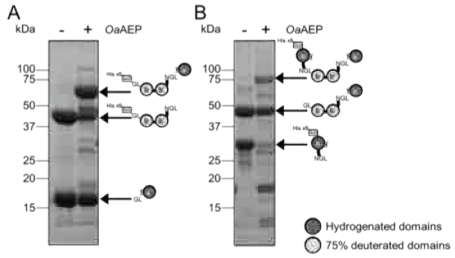

Fig. 1. The ligation products from (A) (*h*)**a'** and (*d*)**bb'** domains and (B) (*h*)**a** and (*d*)**bb'**-(*h*)**a'** domains of ER-60 by *Oa*AEP.

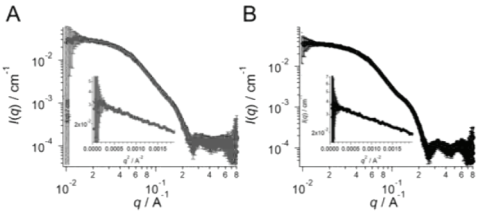

Fig. 2. The SAXS profiles of (A) (*h*)**a**-(*d*)**bb'**-(*h*)**a'** and (B)WT ER-60. the radius of gyration (R_g) of these are 32.8 ± 0.4 Å and 32.0 ± 0.2 Å, respectively. Inset panels are guinier plots of them.

RESULTS: The progress of the first-step ligation reaction, (d)**bb'** and (h) **a'**, and the second-step liga-tion reaction , (h)**a** and (d)**bb'**-(h)**a'**, were observed, indicating that ER-60 with hydrogenated **a** and **a'** domains and deuterated **bb'** domains was pre-pared (Fig. 1). In the SAXS profiles of (h)**a**-(d)**bb'**-(h)**a'** and WT ER-60 showed no significant differences between each other (Fig. 2). Currently, we are proceeding with SANS experiments and analysis of these samples.

REFERENCES:

[1] A. Okuda *et al.,* Sci Rep., **11** (2021) 5655.
[2] M. Sugiyama *et al.,* J. Appl. Cryst, **47** (2014) 430-435.
[3] A. Okuda *et al.,* Angew Chem Int Ed Engl., **62** (2023) e202214412.
[4] A. Okuda *et al.,* Biophys Physicobiol., **18** (2021) 16-27.

CO6-26

^{10}B-enriched nitroimidazole derivative as a functional drug for hypoxia-targeting boron-neutron capture therapy

K. Tanabe,[1] T. Nishihara,[1] T. Ozasa[1] and M. Suzuki[2]

[1]Department of Chemistry and Biological Science, College of Science and Engineering, Aoyama Gakuin University
[2]Institute for Integrated Radiation and Nuclear Science, Kyoto University

INTRODUCTION: Boron neutron capture therapy (BNCT) is a well-known radiation therapy based on the nuclear reaction between boron 10 (^{10}B) atoms and thermal neutrons. BNCT is an ideal cancer treatment, however, this therapy relies on finding boron-containing drugs that are selectively taken up by cancer cells. In particular, applications of therapeutic BNCT for hypoxic cells are slow and therefore, their use is an urgent issue. These research contexts prompted us to prepare a novel drug that could be used to treat hypoxic cells and tumor hypoxia by BNCT. We attempted to modify ^{10}B-enriched p-boronophenylalanine (BPA), a BNCT agent in practical use, for treatment of hypoxic cells. We designed a BPA with nitroimidazole unit (BPA-NI) as hypoxia-targeting BNCT agent (BPA-NI, Fig 1), since nitroimidazoles (NIs) are known as an exogeneous marker for hypoxia because of its characteristic reactions in hypoxic cells. Herein, we characterized the selective accumulation of BPA-NI into hypoxic cells and its cytotoxic effect upon thermal neutron irradiation.[1]

****

EXPERIMENTS: The BPA-NI (0 or 250 μM) was administered to the SAS cells and then the cells were incubated for 3 h. After incubation and wash, the cells were irradiated (neutron, 1 MW) for 45 min at KUR. After incubation, WST 8 was added to the cells, and the cell viability assay was performed using Microplate Reader.

****

RESULTS: We selected SAS cells for the target, because of their versatility for BNCT study, and initially, we checked the intracellular accumulation of BPA-NI. It was well-documented that azomethine H formed chelate complexes with boric acid to exhibit an absorption around 400 nm. Using these characteristic absorption of azomethine H and boron compounds, we attempted to compare the amount of BPA-NI in hypoxic or aerobic cells by the measurement of absorption spectra. After incubation of hypoxic or aerobic cells with BPA-NI, cell lysates were harvested. Then, we added azomethine H to the lysate to measure the absorption spectra. We found that absorption at 420 nm from hypoxic cells was stronger than that from aerobic cells, indicating that BPA-NI selectively accumulated in hypoxic cells. We also measured ICP MS and estimated the amount of ^{10}B element in hypoxic cells to be 78 ng per 10^6 cells. Next, we evaluated the cytotoxic effect of BPA-NI upon thermal neutron irradiation. The cells were incubated with BPA-NI (250 μM) for 3 h under hypoxic or aerobic conditions and then, the cells were subjected to irradiation. We found that the cytotoxic activity of BPA-NI against aerobic SAS cells is negligible, while BPA-NI incubated with hypoxic cells showed higher cytotoxic effect than that with aerobic cells. We also confirmed that the nitroimidazole derivative without BPA unit (A-NI) did not show any cytotoxicity. These results strongly indicate that BPA-NI accumulated in hypoxic cells to show selective cytotoxicity.

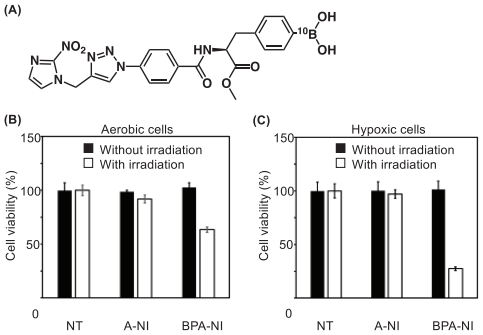

Fig. 1. (A) Chemical structure of BPA-NI. ((B) Cytotoxicity of A-NI and BPA-NI against SAS cells upon thermal neutron irradiation under aerobic (B) or hypoxic conditions (C).

REFERENCES:

[1] K. Tanabe *et al.,* Results Chem., 2025, in press.

CO6-27

Evaluating the Efficacy of Boron Neutron Capture Therapy in Treating Metastatic Central Nerveous System Tumors

Y. Fujikawa, S. Kawabata, H. Yamada, F. Takagi, K. Eza, H. Kashiwagi, T. Takata[1], H. Tanaka[1], M. Suzuki[1], N. Hu[2], S-I. Miyatake[2], T. Takami, and M. Wanibuchi

Department of Neurosurgery, Osaka Medical and Phar maceutical University
[1] Institute for Integrated Radiation and Nuclear Science, Kyoto University
[2] Kansai BNCT Medical Center, Osaka Medical and Pharmaceutical University

INTRODUCTION: With the remarkable progress in cancer treatment in recent years, the life expectancy of patients with cancer has been extended. On the other hand, the risk of developing metastases including spine or central nervous system are increasing. Moreover, the future challenge will be to extend the prognosis and improve the quality of life of patients with metastases [1]. If it could be shown that boron neutron capture therapy (BNCT), which can selectively destroy cancer cells, is effective, it will be a promising novel treatment option and could also contribute to expanding the application of BNCT. Our laboratory has been conducting research on BNCT mainly for malignant brain tumors such as glioblastoma [2,3]. In this study, we aimed to evaluate the efficacy of BNCT for metastatic cancer rat models.
****

EXPERIMENTS: Rat metastatic brain and spine tumor models were created using 13762 MAT B III rat mammary cancer cells. A solitary metastatic brain tumor model was created to be implanted this tumor cell line into the right brain of the rat through the infusion pump. In addition, a multiple metastatic brain tumor model was created to be injected this cell line into the right internal carotid artery of the rat. Finally, metastatic spine tumor model was created by transplanting subcutaneous tumor mass into the vertebral body of the rat. The rat metastatic tumor models were randomly assigned into three groups: a control group receiving no treatment (untreated), a group subjected to neutron irradiation alone (neutron only), and a BNCT group (The BNCT group received an intravenous injection of BPA at a dose of 250mg/kg, followed by neutron irradiation 2.5 h later). In terms of spine metastasis, Overall survival and any adverse events were assessed post-irradiation.
****

RESULTS: BNCT significantly prolonged overall survival in both solitary and multiple brain metastatic tumor rats. In spine metastasis, BNCT group did not have the superior survival compared to the other groups. However, BNCT group with light hindlimb paresis or no paresis (Basso-Beattie-Bresnahan score more than 16) had significant survival prolongation compared to the other groups.
****

CONCLUSIONS: Our data suggests that BNCT is an effective treatment modality for metastatic central nervous system tumors. Further research is warranted to strengthen the evidence supporting the potential benefits of BNCT for these cancers and to facilitate its translation into clinical practice.
****

REFERENCES:
[1] Y. Fujikawa *et al.,* Cancer Sci., **115** (2024) 2774-2785.
[2] K. Tsujino *et al.,* Neurooncol Adv., **22** (2024) vdae062.
[3] Y. Fujikawa *et al.,* Biology (Basel)., **15** (2023) 1240.

CO6-28

Investigation of the Biological Impact of Ultra-High Dose Rate Radiation on Normal and Neoplastic Tissues

Tsubasa Watanabe[1], Genki Edward Sato[1], Takushi Takata[2], Yoshinori Sakurai[2], Minoru Suzuki[1], Takashi Mizowaki[3], Hiroki Tanaka[2]

Institute for Integrated Radiation and Nuclear Science, Kyoto University
[1]Particle Radiation Oncology Research Center, Particle Radiation Oncology
[2]Particle Radiation Oncology Research Center, Particle Radiation Medical Physics
[3]Kyoto Univeristy, Department of Radiation Oncology and Image-Applied Therapy

INTRODUCTION: Recent studies suggest that ultra-high dose rate irradiation (≥40 Gy/sec), which is over 1,000 times faster than conventional radiotherapy (≈0.03 Gy/sec), may reduce side effects while maintaining comparable anti-tumor efficacy [1]. If ultra-high dose rates indeed suppress side effects without compromising anti-tumor effects, conventional radiotherapy (e.g., X-rays, γ-rays, protons) may transition to this approach. Specifically, this year we investigated the functional (rather than quantitative) effects of irradiation on immune cells. Additionally, this project seeks to identify optimal radiotherapy approaches from a tumor immunology perspective. Prior to this year, we analyzed how irradiation affects lymphocyte survival rates and immune function.

****

EXPERIMENTS: We aim to clarify the effects of high-dose rate irradiation—which exhibits distinct biological responses compared to conventional X-ray irradiation—on lymphocytes. First, we established in vivo/in vitro irradiation systems for high-dose-rate exposure using electron beams. Next, we administered high-dose-rate irradiation to the head and neck regions of C3H and C57/BL6 mice, confirming that dermatitis in the high-dose-rate group was reduced compared to the conventional dose-rate group, consistent with published reports. Furthermore, lymphocytes isolated from the spleens of C3H mice were irradiated with 0, 2, 4, and 10 Gy using both conventional and high-dose-rate methods. Based on literature indicating the critical role of oxygen concentration in high-dose rate effects, irradiations were conducted under in vitro conditions with varying oxygen levels. Subsequently, using 5% oxygen conditions (validated for high-dose rate effects in mouse skin), additional irradiations of 0, 4, and 10 Gy were performed under both 1% and 5% oxygen conditions.

****

RESULTS: High-dose-rate irradiation to the head and neck regions of C3H and C57/BL6 mice confirmed that dermatitis was reduced in the high-dose-rate group compared to the conventional dose-rate group, consistent with prior reports. Under 0.1% oxygen conditions, no difference in lymphocyte survival rates was observed between high-dose-rate and X-ray irradiation, and no high-dose rate effect was detected at this oxygen level. Using 5% oxygen conditions (previously validated for high-dose rate effects in mouse skin), 0, 4, and 10 Gy irradiations were repeated under both 1% and 5% oxygen levels. However, under all conditions, no irradiation method-dependent differences in lymphocyte survival rates were observed, and in vitro experiments showed no high-dose rate effect regardless of oxygen concentration.

****

REFERENCES:

[1] JD Wilson *et al.*, Front Oncol., (2020) (doi)10.3389/fonc.2019.01563.

CO6-29

Interaction between fibrinogen and amyloid β 1-42 monitired by analytical ultracentrifugation (AUC

Naoki Yamamoto, Ken Morishima[1], Rintaro Inoue[1], Masaaki Sugiyama[1]

Division of Biophysics, Physiology, Schoolof Medicine, Jichi Medical University
[1]Institute for Integrated Radiation and Nuclear Science, Kyoto University

INTRODUCTION: Fibrinogen is a plasma protein functioning for blood clotting. It has been known that the protein possesses chaperone-like function as it inhibits amyloid fibril formation of several proteins [1-3]. We have recently found that the protein also inhibits amyloid fibril formation of amyloid β 1-42 (Aβ42) which is considered to be a cause of Alzheimer's disease [4]. To understand molecular mechanisms of the inhibition, we evaluated the interaction between fibrinogen and Aβ using AUC.

EXPERIMENTS: Aβ42 at 20 μM was incubated with fibrinogen at 37 °C for 1 hour, followed by AUC experiments using a ProteomeLab XL-I analytical-ultracentrifuge (Beckman Coulter, Germany) with an aluminum cell with a volume of 400 μl (optical path: 12 mm). Bovine and human fibrinogen (bFg and hFg, respectively), which are homologous to each other, were used to investi-gate the effect of the difference in the amino acid sequences.

RESULTS: Figure 1 shows the AUC profiles of Aβ42 in the presence of bFg (A) or hFg (B), respectively. Aβ42 retains two peaks at 0.99 S and 4.53 S, corresponding to the monomer and oligomer, respectively. In the presence of bFg of 3 μM, both peaks disappeared, indicating that bFg interacts with these components. When the concentration was 0.3 μM, the peak of the oligomer was still absent, indicating that bFg interacts with the oligomer more strongly than the monomer. In the presence of hFg of 3 μM, the oligomer peak only disappeared, indicating that hFg only interacts with the oligomer at the concentration. These results represent that bFg possesses higher capabilities for the interaction with Aβ42. This might be due to the difference in their amino acid sequences since bFg and hFg possess similar three dimensional structures.

REFERENCES:

[1] Tang *et al.*, Biochem. Biophys. Res. Commun., **378** (2009) 662-667.
[2] Swasthi *et al.,* Biochemistry. **57(44)** (2018) 6270-6273.
[3] N. Yamamoto *et al.,* J. Phys. Chem. B, **126(51)** (2022) 10797-10812.
[4] Manuscript submitted

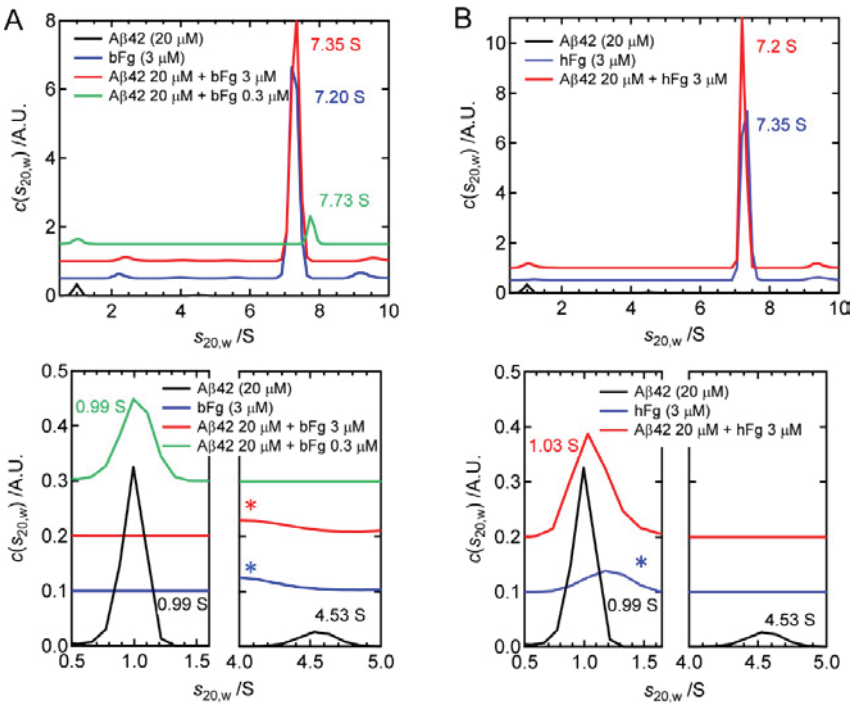

Fig. 1. AUC profiles of Aβ in the presence of bFg (A) or hFg (B), respectively. The top panels show total profiles and the bottom panels are magnified views of the low-S regions corresponding to Aβ42 monomer and oligomer, respectively.

CO6-30

Radiolabeling of composite natural material chicken eggshell membrane via neutron irradiation 6Li(n,α) 3H reaction

M. Shimizu[1], E. Ohto-Fujita[1], N. Nogawa[2], H. Yoshinaga[3], K. Takamiya[3], A. Enomoto[4], K. Tanoi[5], T. Yamashita[6], Y. Asano[7], Y. Hasebe[8], and Y. Atomi[1]

[1]*Teikyo University, Advanced Comprehensive Research Organization, Division of Open Innovation*
[2]*Isotope Science Center, The University of Tokyo*
[3]*Institute for Integrated Radiation and Nuclear Science, Kyoto University*
[4]*Isotope Facility, Graduate School of Medicine, The University of Tokyo*
[5]*Isotope Facility for Agricultural Education and Research. Graduate school of Agricultual and Life Sciences, University of Tokyo.*
[6]*Department of dermatology, Graduate School of Medicine, The University of Tokyo*
[7]*Department of Dermatology, Tohoku University Graduate School of Medicine*
[8]*Almado, Inc.*

INTRODUCTION: Chicken eggshell membrane (ESM) has been listed as an excellent wound-healing agent in Chinese pharmacopoeia book entries for 400 years. It is a non-woven fabric composed of more than 400 fibrous protein polymers, cross-linked by lysyl-oxidase [1]. We previously found that hydrolyzed ESM provide young extracellular environment to dermal fibroblast [2] , improved skin elasticity and reduced facial wrinkles as cosmetics [3] and improved skin elasticity, respiratory function, and locomotion in healthy adults taking the supplements [4]. Recently, we also reported the potential of ESM and its key components, lysozyme (LYZ) and ovotransferrin (OT), as a promising preventive approach for pulmonary fibrosis [5]. We applied the tritium labeling of organic compounds via the 6Li(n,α)3H reaction, which has been used for radiolabeling of natural products that are difficult to synthesize and for tissue distribution in individuals, to ESM and conducted pilot experiments to determine whether ingested ESM are indeed digested and absorbed and distributed to various tissues. The labeled eggshell membrane was orally administered to mice and was digested and absorbed. The radioactivity derived from the labeled ESM was detected in blood 2 hours after administration, peaking 6 hours later, and was also detected in almost all tissues [6]. The Kyoto University furnace is beneficial for irradiating protein samples because its low power output does not raise the sample temperature during irradiation.
****

EXPERIMENTS: ESM (nano-sized extra-fine form, Almado Inc.) + Li_2CO_3 (1:1 and 1:2 by weight) and SESM (solubilized ESM form, Almado Inc.) + Li_2CO_3 (1:1 and 1:2 by weight) sealed in quartz glass were irradiated under milder conditions (Pn-2, 1 MW, 70 min). After irradiation, samples were transferred to The University of Tokyo for biochemical, in vitro, and in vivo study.
****

RESULTS: The chemical integrity of the protein after Pn-2 irradiation and the peptide size after digestion and absorption into the serum and mouse tissues will be determined using SDS-PAGE and peptide gel. Using cell line, uptake of labeled protein and secretion of ECM (decorin, type III collagen, MMP2) will determine the biological activity of the irradiated protein sample.
****

REFERENCES:

[1] M. Shimizu *et al.*, The journal of Japan Mibyou Association, **30** (2024) 23-26.
[2] E. Ohto-Fujita *et al.*, Cell Tissue Res., **345** (2011) 177-190.
[3] E. Ohto-Fujita *et al.*, Cell Tissue Res., **376** (2019) 123-135.
[4] E. Ohto-Fujita *et al.*, Journal of Fiber Science and Technology **77** (2021) 258-265 . 115-120.
[5] E. Ohto-Fujita *et al.*, Biochem. Biophys. Rep. 2024, **39** (2024) 101806 .
[6] E. Ohto-Fujita *et al.*, Journal of Fiber Science and Technology, **77** (2021) 182-187.

CO6-31

Solution structure of VAMP722

K. Kato[1,2,3], M. Yagi-Utsumi[1,2,3], H. Yagi[1,2], K. Morishima[4], R. Inoue[4] and M. Sugiyama[4]
[1]*Graduate School of Pharmaceutical Sciences, Nagoya City University*
[2]*Exploratory Research Center on Life and Living Systems (ExCELLS), National Institutes of Natural Sciences*
[3]*Institute for Molecular Science, National Institutes of Natural Sciences*
[4]*Institute for Integrated Radiation and Nuclear Science, Kyoto University*

INTRODUCTION:

VAMP721 (vesicle-associated membrane protein 721) is a plant-specific R-SNARE protein that plays a crucial role in vesicular trafficking to the plasma membrane, where it mediates membrane fusion events essential for polarized secretion and cell expansion. AlphaFold-based structural modeling predicts that VAMP721 adopts a "closed" conformation, in which its SNARE motif folds back onto the N-terminal longin domain, potentially representing an autoinhibited state. In contrast, docking models of VAMP721 in complex with the clathrin adaptor PICALM suggest an "open" conformation, where the SNARE motif is extended and accessible for interaction, implying a possible mechanism of conformation-dependent regulation of protein–protein interactions.

To investigate the conformational state of VAMP721 in solution, we employed small-angle X-ray scattering (SAXS) and analytical ultracentrifugation (AUC). These complementary biophysical techniques provide insights into the overall shape, oligomeric state, and conformational dynamics of VAMP721 under physiological conditions, enabling us to assess whether it predominantly adopts a closed, open, or intermediate ensemble of conformations in solution.

EXPERIMENTS:

Recombinant VAMP721 was expressed in Escherichia coli and purified using GST affinity chromatography. The protein was dissolved in buffer containing 20 mM Tris-HCl (pH 8.0) and 150 mM NaCl. SAXS measurements were performed at 25 °C using a NANOPIX instrument (Rigaku) installed at KURNS. Scattering data were collected over a q-range of 0.010–0.70 Å^{-1} using two sample-to-detector distances (SDDs) of 1333 mm and 300 mm. To minimize the influence of non-specific aggregation on the SAXS profiles, we applied the AUC-SAXS method, an integrated reduction approach combining analytical ultracentrifugation (AUC) and SAXS. AUC measurements were conducted using a ProteomeLab XL-I (Beckman Coulter) at 60,000 rpm and 25 °C.

RESULTS:

Figure 1B shows the experimental SAXS profile of recombinant VAMP721. The scattering curve was compared with theoretical profiles derived from the AlphaFold-predicted closed model and the open conformation observed in PICALM docking simulations. Fitting analysis indicated that VAMP721 exists as a dynamic equilibrium of conformers in solution, comprising approximately 57% open and 43% closed states. These results suggest that VAMP721 samples both conformations in the absence of binding partners, reflecting conformational flexibility that may underlie its regulatory mechanism in vesicle trafficking.

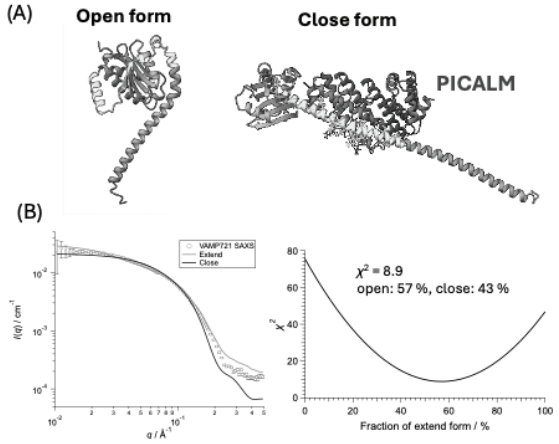

Fig. 1. Solution structure of VAMP721 compared with predicted structural models.
(A) Predicted "closed" and "open" conformation of VAMP721 generated by AlphaFold.
(B) Experimental SAXS profile of recombinant VAMP721 (black dots) compared with theoretical scattering curves calculated from the closed (blue) and open (red) models. The experimental data show better agreement with a possible mixture of conformational states in solution.